

72320 Roversystemtechnik
Summer Semester 2021

INSPIRE

IN-situ Sampling and Primal Investigation Rover on Europa

**Phase 0/A-Study of a Rover Mission on the Surface
of the Jupiter moon Europa**



Denis Acker
Daniel Bölke
Korbinian Kasper
Christian Korn
Nicolas Probst
Saskia Süitterlin

Supervisors:
Moritz Nitz M.Sc.
Patrick Winterhalder M.Sc.

University of Stuttgart
Institute of Space Systems
Prof. Dr. Sabine Klinkner
18.07.2021

Symbols

Symbol	Definition	Unit
a	Constant for the Geometry of a Porous Media	nm
A	Wheel Ground Contact Area	m
b	Wheel Width	m
c	Coefficient of Soil Cohesion	Pa
$C_{\text{batt},\text{req}}$	Total Required Battery Capacity	Wh
$C_{\text{batt},\text{nom}}$	Battery Nominal Capacity	Wh
C_{cell}	Cell Voltage	V
CON_*	Heat conductance of concerning component	$\frac{W}{K}$
C_{rr}	Rolling Resistance Coefficient	-
d	Wheel Diameter	m
DoD	Depth of Discharge	%
DP	Drawbar Pull	N
H	Soil Thrust	N
h_{ice}	Ice Crust Surface Thickness on Europa	m
k_c	Sinkage Modulus	$\frac{kN}{m^{n+2}}$
k_ϕ	Soil Friction Angle Sinkage Modulus	$\frac{kN}{m^{n+3}}$
l	Ground Contact Length	m
R_t	Heat resistance	$\frac{K}{W}$
T_{surface}	Surface Temperature on Europa	K
M	Number of Cells in Parallel	-
m_{RTG}	RTG Mass	kg
m_w	Weight per Wheel	kg
n	Soil Deformation Exponent	-
N	Number of Cells in Series	-
P_{el}	RTG Electrical Power	W_{el}
$P_{\text{el},\text{req}}$	Required Electrical Power	W_{el}
P_{mode}	Demanded Electrical Power per Mode	W_{el}
\dot{Q}	Heat flow	W
S_0	Solar constant	$\frac{W}{m^2}$
R_b	Bulldozing Resistance	N
R_c	Compaction Resistance	N
R_g	Gravitational Resistance	N
R_r	Rolling Resistance	N
S	Radiation surface	m^2
t_e	Mode Duration	s
W_{wheel}	Normal Force per Wheel	N

SYMBOLS

z	Sinkage	m
α	Absorptivity	-
α_{BOL}	BOL Specific Power	$\frac{W_{el}}{kg}$
δ_R	Ecliptic latitude of the rover on Europa	o
ϵ	Emissivity	-
η_{LiIon}	Efficiency of LiIon Cells	-
λ	Heat conductivity	$\frac{W}{mK}$
λ_R	Ecliptic longitude of the rover on Europa	o
ϕ	Friciton Angle	o
φ	View factor	-
ρ_E	Albedo of Europa	-
ρ_{ice}	Inner Encoder Ring Diameter	$\frac{kg}{m^3}$
σ_b	Stefan-Boltzmann constant	$\frac{W}{m^2 K^4}$
θ	Slope Angle	o

Abbreviations

2D	Two Dimensional
3D	Three Dimensional
BOL	Begin of Life
BOM	Begin of Mission
COMM	Communications
C&DH	Command & Data Handling
CPU	Core Processing Unit
DoD	Depth of Discharge
EOM	End of Mission
EPS	Electrical Power System
FEC	Forward Error Correction
GPR	Ground Penetrating Radar
HGA	High Gain Antenna
IRS	Institute of space Systems at the University of Stuttgart
INSPIRE	IN-situ Sampling and Primal Investigation Rover on Europa
JUICE	Jupiter Icy Moons Explorer
LGA	Low Gain Antenna
PCDU	Power Control and Distribution Unit
PCU	Power Control Unit
PDU	Power Distribution and Control Unit
IMU	Inertial Measurement Unit
ESA	European Space Agency
MMP	Mean Maximum Pressure
MP	Mobility Package
NASA	National Aeronautics and Space Administration
SPENVIS	SPace ENVironment Information System
HPC	High Priority Commands
RHU	Radioisotope Heater Unit
RTG	Radioisotope Thermoelectric Generator
eMMRTG	Enhanced Multi Mission Radioisotope Thermoelectric Generator
eSMMRTG	Enhanced and Scaled Multi Mission Radioisotope Thermoelectric Generator (3kg)
TID	Total Ionizing Dose
TRIPLE	Technologies for Rapid Ice Penetration and Subglacial Lake Exploration
TRL	Technology Readiness Level
OBC	On-Board Computer
S/C	Spacecraft
SBC	Single Board Computer

Contents

Symbols	I
Abbreviations	III
List of Figures	VII
List of Tables	VIII
1 The Mission	1
2 Payload	2
2.1 Ground RADAR	2
2.2 Ice Core Drill	2
2.3 APXS Analyzer	3
2.4 Sterovision Camera / Observation / Perception	3
2.5 RadHard Solar Arrays	3
3 Operation	4
3.1 Scientific Output	4
3.2 Rover System Modes	5
4 Subsystems	7
4.1 Structure and Mechanisms	7
4.1.1 Storage Configuration and Rover Deployment	7
4.1.2 Exploration Configuration	7
4.1.3 Static Analysis	7
4.1.4 Mass Budget	7
4.2 Locomotion	8
4.2.1 Design Drivers for Rover Classification	8
4.2.2 System Parameters	8
4.2.3 Deployment mechanism	11
4.3 Electrical Power System	11
4.3.1 EPS Budget and Overview	11
4.3.2 Energy Source	12
4.3.3 Energy Storage	13
4.3.4 EPS Power Control and Distribution	14
4.4 Communications and Command & Data-Handling	14
4.4.1 Operational Concept	14
4.4.2 Communication System	14
4.4.3 Command & Data Handling	15
4.5 Thermal Control System	15
4.5.1 Concepts	16
4.5.2 Thermal Network	17
4.5.3 Analysis	18
4.5.4 Results	18
4.5.5 Results	18
4.6 Radiation	19
4.6.1 Radiation Protection	19

4.6.2	Components	20
4.6.3	Improvements	20
4.6.4	Conclusion	20
5	Outlook & Risk Assessment	22
5.1	Risk Assessment	22
5.2	Outlook	22
	Bibliography	23
	Appendix	25
A	Operation	25
B	Structure and Mechanism	26
C	Locomotion	28
	C.1 Locomotion Design Drivers	28
D	Electrical Power System	31
E	Communications	33
	E.1 Link Budget	33
	E.2 Mission Data Output	34
	E.3 Communications Trade Off	36
	E.4 Command & Data Handling Trade Off	36
F	Thermal Controls System	41
	F.1 Heat energy equilibrium	41
	F.2 Heat conductance	43
	F.3 Heat switch	47
	F.4 Rover absorptivity	49
	F.5 Input Values	49
G	Radiation	52
	G.1 Jupiters Radiation Environment	52
	G.2 Radiation Exposures	53
	G.3 Improvements	54
H	Digital Appendix	56

List of Figures

3.1	Preliminary Mission Timeline for INSPIRE.	4
3.2	Timeline of a mission day during phase 4	4
4.1	Wheel sinkage z as a function of the slope angle θ of each configuration with different soil parameters, referred to Figure C.2.	9
4.2	Comparison of the rover's soil thrust versus the motion resistance to exceed, each for the soil parameters of snow in Sweden and heavy clay, referenced to Figure C.2.	10
4.3	Functional Flow Chart Diagram for the EPS Subsystem.	11
4.4	Functional Flow Chart Diagram for the EPS Subsystem.	12
4.5	Carbon-based thermal strap <i>LyNX®</i>	16
4.6	Bi-metallic heat switch, [20].	16
4.7	Change of the heat switch conductivity R_t over the mean temperature T_M	17
4.8	Thermal network of the rover.	17
4.9	Overview of TIDs within different compartments within the rover.	21
C.1	Trade-off of the locomotion movement system. The criteria with the respective weighting factors are shown on the left. On the right side are the respective systems.	28
C.2	Soil Parameters	28
C.3	Various wheel dimensions respective to the weight. Rows highlighted in red are not considered further for system design due to the limit of 200 g weight per wheel.	29
C.4	30
C.5	Parameters for the mean maximum pressure for a wheeled rover.	30
D.1	Holistic Power Budget of INPSIRE.	32
E.1	Rover to Lander complete downlink budget.	34
E.2	Bit Error Rate for different FEC codes	36
E.3	Transmitter Trade off for the Communication subsystem.	37
E.4	Receiver Trade off for the Communication subsystem.	38
E.5	Antenna trade off for the Communication subsystem.	39
E.6	OBC trade off for the Command & Data Handling subsystem.	40
F.1	Conductance characteristic of heat switch diveded in sections.	48
F.2	Bi-metallic heat switch, [20].	49
F.3	Digitalised [17] and calculated heat conduction in comparison.	50
G.1	Average trapped proton and electron fluxes on an orbit around earth at 25,000 km, through the outer Van Allen radiation belt, and on Europa's orbit around Jupiter.	52
G.2	TID of aluminium, titanium, and the optimised radiation structure shown in Table 4.8 with a weight target of all three structures of 0.5 g/cm^2 over 30 days of exposure on Europa.	53
G.3	TID for different compartments as seen in Figure 4.9. The E-Bay is shielded by 4 mm aluminium, 0.415 mm lead, and 0.033 mm iron; the camera compartment by 2 mm aluminium, 0.415 mm lead, and 0.033 mm iron; the chassis by 2 mm aluminium; the electric motors by 1 mm aluminium.	53
G.4	TID with 4 mm Al shielding over a mission duration of 30 days	55
G.5	TID with 4 mm Al shielding and 1 cm of Water over a mission duration of 30 days	55

List of Tables

2.1 GPR antenna properties	2
3.1 Expected scientific data output of the INSPIRE mission	5
4.1 Fundamental rover design and the respective design drivers.	8
4.2 Configurations for rover classification respective to the wheel width bw , wheel diameter d_w and weight per wheel m_w	9
4.3 Parameters for the scaled eSMMRTG based on the eMMRTG.	12
4.4 Power consumption mode used as design case for the battery sizing.	13
4.5 Key criteria of selected communication components	15
4.6 Temperature results in K of thermal analysis, <i>with out</i> margin	19
4.7 Temperature results in K of thermal analysis, <i>with ±15 K</i> margin	19
4.8 Optimal shield structure for an Jupiter mission. [Platzhalter]	20
5.1 Subsystem TRL for risk assessment	22
A.1 Collection of Rover System Modes.	25
B.2 INSPIRE Mass Budget	27
C.1	29
D.1 INSPIRE battery parameters.	31
E.1 Transmission link parameters	33
E.2 Complete link budget for Lander to Rover (L2R) transmission.	35
E.3 Comparison of transmission times per image (message frame bits included)	37
E.4 Transmission time and total data output per mission day	37
F.1 Definition of heat conductance C between the nodes according to Figure 4.8.	43
F.2 Definition of heat conductance $CON = \frac{1}{R}$ between the nodes according to Figure 4.8. .	44
F.3 Definition of heat conductance $CON = \frac{1}{R}$ between the nodes according to Figure 4.8. .	45
F.4 Definition of heat conductance $CON = \frac{1}{R}$ between the nodes according to Figure 4.8. .	46
F.5 Definition of heat conductance $CON = \frac{1}{R}$ between the nodes according to Figure 4.8. .	47
F.6 Sections and range of the switch characteristic.	48
F.7 Toggle temperature and amount of bi-metallic heat switch.	48
F.8 Temperatur limits of the rover components.	49
F.9 Dimensions of the thermal straps <i>LyNX®</i>	50
F.10 Minimum and maximum of surface emisivity and absorptivity values, [21].	51
F.11 Heat conductivity in $\frac{W}{mK}$	51
F.12 Radiation surface and finishing of components.	51
G.1 Used components and the respective radiation tolerance and location	54
H.1 Digital Appendix	56

Chapter 1

The Mission

During the observation of Jupiter, the Galileo spacecraft performed flybys of the Jupiter moons, [1]. The scientist gathered data from Europa, which supported the evidence of a thick icy surface. The possibility of liquid water underneath lead astrobiologists to the assumption that extraterrestrial life could exist on Europa, [2]. That is why Europa is - beside Mars - an interesting object of research.

Therefore, the ESA will launch the *JUICE* orbiter in 2022 to investigate Europa in more detail, [3]. But also the NASA is developing *Europa Clipper* to get detailed information. Additionally, they plan a lander for Europa to bring scientific instruments onto the surface, [4] [5].

Under the leadership of Prof. Dr.-Ing. Klinkner, the Institute of Aero Space Systems started within a seminar a feasibility study about a rover system to explore Europa surface, which shall be part of the *TRIPLE* mission. This challenge was given to five student teams in order to develop concepts, construct preliminary designs, perform analysis and make evaluations to meet the mission objectives and fit the mandatory requirements cite.

This report contains the results of the Phase A study of the rover system IN-SITU SAMPLING AND PRIMAL INVESTIGATION ROVER ON EUROPA (INSPIRE).

Chapter 2

Payload

The Main Payload (Ground Radar, Ice Core Drill and APXS sensor) as well as the secondary payloads (Cam Head and Rad Hard Solar cells) will be explained in Detail in this Chapter.

2.1 Ground RADAR

The Ground Radars main task is the identification of suitable drilling sites. Additionally every radar campaign will contribute to further understanding of the ground composition on Europa.

due to its small dimensions the CRUX GPR is selected . The system is tested for lunar application at 800 MHz resulting in a resolution of 15 cm and a penetration depth of 5 m [CRUX RADAR REF]. The INSPIRE mission makes use of a 1.5 GHz frequency to increase the resolution.

Reduced penetration depths are acceptable since the depth of interest for the ice core sampling is 10 cm.

Additionally high frequencies lead to compact antenna design which is beneficial to the INSPIRE mission due to weight constraints. Based on [Paper & Website reference] a custom patch antenna with the properties in Table 2.1 is proposed.

Substrate ϵ_r	Width	Length	Height	Mass
20	30 mm	20 mm	2 mm	2,73 g

Table 2.1: GPR antenna properties

2.2 Ice Core Drill

The ice core drill is an in-house development which is based on the NanoDrill from Honeycomp and the drill from Philae. The drill is made of titanium to ensure that it does not deform or even break through during the drilling process. The ice core sample that can be obtained has a length of 100 mm and a diameter of 10 mm In order to save space, the drill is folded in while driving and is then unfolded in the "Payload: IceCoreDrill" mode, which is illustrated in the following figures. (PICTURE) When the drilling process is finished, it is folded in again and the trap doors are closed. Now the sample can be pushed out with the help of a plunger and meanwhile it can be analyzed by the APXS sensor. (Figure XXX)

APXS SENSOR

When the sample has left the drill body and the analysis is complete, the rover can switch back to Locomotion mode and look for a new place to drill. As soon as a new drilling process is started, the previously taken sample falls to the ground at the same time to make room for a new one.

2.3 APXS Analyzer

...

2.4 Sterovision Camera / Observation / Perception

The INSPIRE rover is equipped with five individual cameras. Two are used as stereo vision cameras on an hight adjustable and rotatable telescope arm on the front side of the rover. This ist used to capture a detailed 3D model of the environment with which sizes and distances can be estimated. The remaining three cameras are used as has-cameras which are necessary to obtain data regarding the nearby environment. All cameras are equipped with radiation hardened lenses to prevent browning of the lenses. The main tasks of the camera system is the provision of scientific data and navigation related data. More details regarding the navigation and autonomy are provided in ??.

2.5 RadHard Solar Arrays

As a secondary mission goal for INSPIRE a cooperation with the european project RadHard which is led by the german solar array manufacturer Azure Space is intended. They are currently developing a new generation of 4 Junction solar cells with an efficiency of up to 35 %. But the main feature of the new solar arrays is their radiation hardness which will be the highest radiation hardness ever designed with an efficiency of $> 3\%$ after $1E15 \text{ cm}^{-2}$ 1 MeV electron irradiation. So the Jupiter environment with its extreme radiation would be the best suitable destination for a test and evalauation mission of this new technology. Therefore INSPIRE will be equipped with 8 RadHard solar cells with a total surface area of 0.0248 m^2 for a technology demonstration [6].

Chapter 3

Operation

For the INSPIRE Mission Phase 0 study five basic mission phases have been defined. Nominal mission will last 30 earth days which is equal to 8.47 European days (MISSING REFERENCE). Furthermore a sixth optional mission phase after the nominal mission lifetime has been established which will be conducted if the rover is still operational after its nominal lifetime.

- **Phase 0:** Launch and Flight Phase
- **Phase 1:** Entry, Descent and Landing Phase
- **Phase 2:** Deployment Phase
- **Phase 3:** Egress, Commissioning and Early Operation Phase
- **Phase 4:** Mission Operation Phase
- **(Phase 5:** Exceeding Mission Operation Phase)

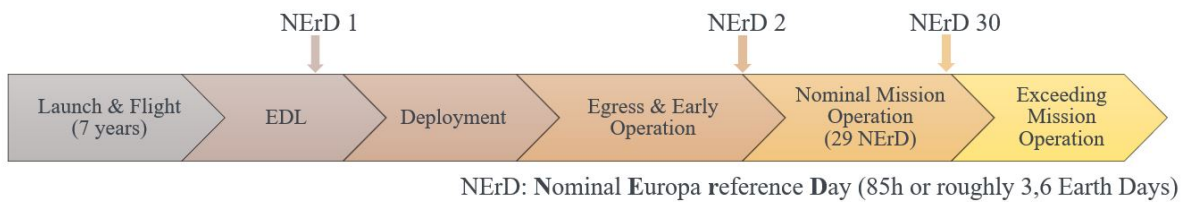


Figure 3.1: Preliminary Mission Timeline for INSPIRE.

Based on these missions phases some preliminary rover system modes as well as a basic mission timeline were concluded.

3.1 Scientific Output

Optical reference systems for path planning limit operation of the rover to an average of 41 h of sunlight (out of 85 h in a European day). Figure 3.2 depicts a breakdown of possible execution times in a mission day based on the power budget. Of course the given order can be changed and execution times can be adapted to fit the mission needs.



Figure 3.2: Timeline of a mission day during phase 4

Locomotion phases consist of a sequence of mobility packages (MP). Each MP is built up of 5 min path planning and 10 s driving. Path planning time is estimated based on the limited

processor speed.

Within the 6 h of a single Locomotion phase, a distance of 68 m is covered, resulting in a maximum distance of 1.7 km for the nominal mission.

With respect to the payloads of the INSPIRE mission described in Chapter 2 the scientific return for phase 4 will consist of the data in Table 3.1. Out of the 9 h of payload operation a total of 6 h is used for imaging and radar measurements.

The total data output can be increased further in the case of a sufficient power margin during operation.

Table 3.1: Expected scientific data output of the INSPIRE mission

Payload	Data Output	Data Output
GPR	raw radar measurements	40
Cameras	grayscale images with optional 3D mapping	>3570 images
Sample Analyser	raw mineral analysis of ice core	10 - 12 samples
Solar Cells	performance data	continuous

3.2 Rover System Modes

For this case study several rover system modes were defined. All ten modes are listed in Table A.1. They are separated into two groups. The design critical modes are displayed in white and are defined as system modes, which significantly influence the preliminary design of the rover subsystem like the thermal or power subsystem. None design critical modes (grey) also have a major influence on multiple subsystems of the rover but play a secondary role in the thermal and power budget of the rover for this Phase 0 study. These non design critical modes extend from the rover storage and launch until the finale deployment of the rover is completed. These modes and their design options depend heavily on the final design of the lander with which INSPIRE flies to Europe. Therefore, a clear definition of such modes is not possible at this time in the course of this phase 0 study. However, the respective considerations, preferences and options have been briefly described in the mode descriptions. It is important to note that INSPIRE's goal is to provide a flexible rover design with as few hard requirements as possible for the parent lander. Therefore, many aspects of the rover, as well as the none design critical modes, will need to be further defined and elaborated in later phases of the project in close consultation with the customer.

For example, the exact interfaces between rover and lander should be defined in more detail. Depending on the subsequently chosen interfaces, many possibilities may arise in the corresponding rover system modes. With an appropriate interface, for example, the excess electrical and thermal energy of the RTG, which is already active during the flight, could be used to supply the lander system with heat and power. A corresponding interface could also enable the transmission of health checks from INSPIRE.

The deployment phase will strongly depend on the final design of the lander, INSPIRE's position within the lander and also the possibilities that the lander provides to INSPIRE. Possible deployment strategies would be as follows:

- **Option 1:** If INSPIRE on ground level: Release from storage box through spring mechanism or actuators. Rover storage configuration allows rolling and possible motorised actuation

3.2. ROVER SYSTEM MODES

- **Option 2:** If INSPIRE is above ground level: Similar as Option 1 but an additional ramp and ramp deployment would be required.
- **Option 3:** INSPIRE will be deployed through the landers robotic arm if it is capable of lifting its mass.

Chapter 4

Subsystems

In this chapter, the individual subsystems of the rover system will be discussed in more detail.

4.1 Structure and Mechanisms

...

4.1.1 Storage Configuration and Rover Deployment

The Main Characteristics of the Rover Chassis design of INSPIRE focuses on compact storage geometry and low Mass. During the design process it's been possible to achieve a reduce of volume in comparison to the first INSPIRE chassis design of about xxx %. The geometry data in storage configuration is shown in figure XXX. The storage volume that is required is 131 l. For the Rover Deployment there had been a lot of possible concepts, for example a sky crane, a robotic arm or a ramp. Depending of the reason that there are no further informations about the TRIPLE Lander and that the complexity of such a deployment system should be as simple as possible, the decision fell on a ramp where INSPIRE will drive slowly downwards the surface of Europa. A possible concept of the rover deployment is shown in the following figure XXX.

4.1.2 Exploration Configuration

When the deployment is successfully done, INSPIRE has to switch from storage - to exploration configuration. This will be possible with a cogwheel mechanism which will be operated by two Motors (QUELLENVERWEIS). When the wheel forks are horizontal to the ground, the rover is ready for its journey. In order to withstand the potential bumps on the moon's surface, a planetary gear differential is installed which should prevent the rover from tipping over by reflecting the pushing force on the other side of the landing gear to ensure ground contact.

4.1.3 Static Analysis

As part of the design process, it was necessary to perform a static analysis of the chassis. The following load cases were considered:

- Stowed configuration inside the TRIPLE lander on Europa
- Exploration configuration on the surface of Europa

The analysis was created with the computer aided design software "Autodesk Inventor". The results of this analysis are shown in the following figures XXX and XXX.

4.1.4 Mass Budget

A really important part of each space system is the mass budget. Due to the strict mass restriction, it was quite difficult to find a suitable concept that is both light and space-saving. In order to make the design process of INSPIRE more effective, a specially selected preferred maximum mass of the chassis with the mechanisms of 5 kg was chosen which could also be adhered to. The following table lists the masses of the individual components of the structure and mechanisms system. A table with all components of the INSPIRE Rover system is stored in Appendix A under Mass Budget.

4.2 Locomotion

The locomotion subsystem deals with the aspect of how the rover moves and the technical design, including the selection of components such as motors or gears. Before the components can be determined, however, it is necessary to consider certain parameters and design drivers. These will be introduced in the following, and the decisions or estimations concerning the rover will be presented.

4.2.1 Design Drivers for Rover Classification

The fundamental rover design can be described by the wheel formula 4x4x4, based on a trade-off, presented in Figure C.1. A more detailed design and the main criteria related to this are summarised in Table 4.1.

Table 4.1: Fundamental rover design and the respective design drivers.

Wheeled System	4-Wheels
One of the most common types of platform - high level of experience - high TRL	Compared to 2-wheels: - stability can be ensured → important for drilling - MMP decreases
Compared to other systems: - analysis quite straightforward - simplification → one of the most critical design drivers	Compared to 6-wheels: - less complex → simplification - mass can be reduced
All-Wheel Drive	All-Wheel Actuation
- traction can be increased - increase of DP and the slope angle θ	- reduces the risk of slippage on ice

Furthermore, the normal force on Europa can be calculated to $W = m_{\text{total}} \cdot g_{\text{Europa}} = 39.45 \text{ N}$. Since each wheel is individually driven and controllable, the parameters in the following are designed for one wheel; the normal force per wheel is correspondingly $W_w = 9.8625 \text{ N}$.

4.2.2 System Parameters

Regarding techniques of rover movement, it is crucial to consider the local conditions in which the rover will be operating. The surface of Europa can be assumed to be mainly covered by ice. However, since there are also geysers that transport water to the surface, surface areas may be covered by snow. Though Europa's surface temperature does not exceed 130 K, rather icy, hard-packed snow can be assumed. For this study, a conservative design of the rover is considered, with soil parameters of snow in Sweden as well as heavy clay as a substitute for a hard ice surface; both are listed in Figure C.2. Furthermore, the parameters depend on the width and diameter of the wheels of the rover. Therefore, several sizes dependent on the respective weight were selected and a limit per wheel was set to 200 g, illustrated in Figure C.3. This constraint results in 6 configurations considered for the Rover system design, listed in Table 4.2.

Trafficability Configuration

The ability of traffic depends on the soil parameters as well as on the geometric dimensions of the wheels. The sinking depth z for each wheel of the rover can be determined to:

$$z = \left(\frac{3W_{\text{wheel}} \cos \theta}{(3-n)(k_c + b_w k_\phi) \sqrt{d_w}} \right)^{\frac{2}{2n+1}}. \quad (4.1)$$

Table 4.2: Configurations for rover classification respective to the wheel width b_w , wheel diameter d_w and weight per wheel m_w .

Configuration	b_w / m	Diameter d_w / m	Weight m_w / kg
1	0.05	0.1	0.127
2	0.06	0.1	0.153
3	0.07	0.1	0.178
4	0.05	0.125	0.154
5	0.05	0.125	0.185
6	0.05	0.15	0.185

As shown in Figure 4.1, the sinking depth z depends not only on the geometric conditions and soil parameters but also on the slope angle θ . Therefore, z can be determined for both soils with respect to θ as plotted in Figure 4.1. However, it can be assumed that for the expected soil, the following applies: $z_{\text{Heavy Clay}} \leq z_{\text{Europa}} \leq z_{\text{Snow}}$.

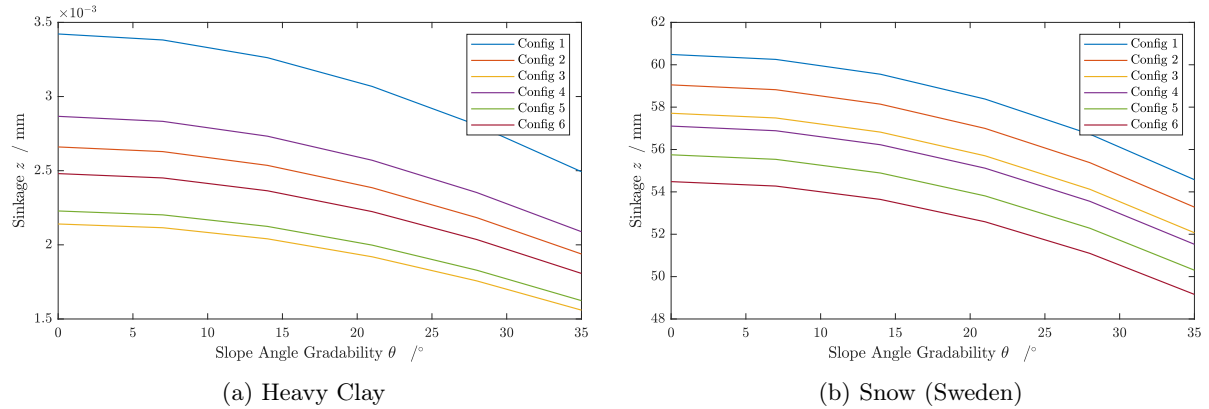


Figure 4.1: Wheel sinkage z as a function of the slope angle θ of each configuration with different soil parameters, referred to Figure C.2.

The required power for the rover can be calculated by the resistances that have to be exceeded. For the total resistance, the following applies:

$$R_{\text{total}} = \underbrace{R_{\text{compaction}}}_{= \frac{z^{n+1}}{n+1} (k_c + b k_\phi)} + \underbrace{R_{\text{rolling}}}_{R_r = W_w C_{rr}} + \underbrace{R_{\text{gravity}}}_{R_g = W_w \sin \theta} + \underbrace{R_{\text{bulldozing}}}_{R_b \rightarrow 0}. \quad (4.2)$$

Due to the hard surface of Europa, it can be assumed that $R_b \rightarrow 0$. In contrast to the R_g , R_r can be defined as constant. With a rolling resistance coefficient of $C_{rr} = 0.02$, the resulting resistance is $R_r = 0.1972 \text{ N}$ [rolling coefficient]. Analogous to z , the lower limit of R_{total} with soil properties of heavy clay is plotted in Figure 4.2c, while the upper limit is shown in Figure 4.2d for snow.

In addition to the resistance that needs to be exceeded in order to move, an upper limit can also be determined. The ground thrust H indicates the maximum amount of traction that can be achieved before the wheels slip. Therefore, following applies:

$$H = A \cdot c + W_w \cdot \tan \Phi, \quad (4.3)$$

with the wheel ground contact area $A = \frac{\pi}{4} \cdot b_w \cdot l$ and the ground contact length $l = \frac{d_w}{2}$.

$\cos^{-1} \left(1 - \left(\frac{2z}{d_w} \right) \right)$. As a result, the absolute upper limit of traction is presented in Figure 4.2a for heavy clay and Figure 4.2b for snow.

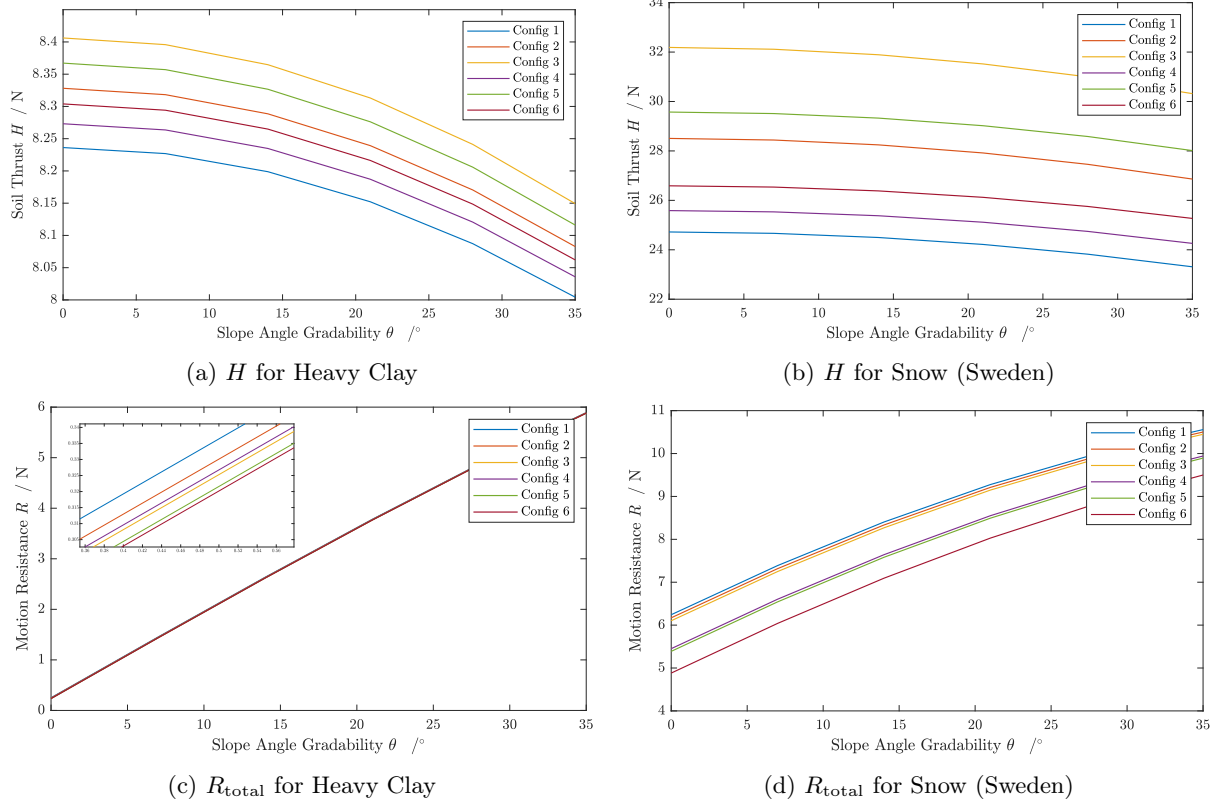


Figure 4.2: Comparison of the rover’s soil thrust versus the motion resistance to exceed, each for the soil parameters of snow in Sweden and heavy clay, referenced to Figure C.2.

In addition to the determined parameters, it should also be verified that the mean maximum pressure MMP does not increase excessively due to the selected geometric parameters. For this conservative calculation, a rigid wheel is assumed, whereby for the deflection δ applies, that $0 \leq \delta \leq 0.1d$. For terrestrial snow, 40 kPa should not be exceeded, but ideally the MMP should be less than 10 kPa. The associated verification calculation can be found in Appendix C.1. For the Rover, configuration 6 is chosen as it offers the lowest resistance to exceed whilst maintaining the lowest MMP .

Steering

Since the rover has an all-wheel actuation, it can be operated with on-point steering and, in order to avoid greater obstacles, with Ackerman steering. Considering that with Ackerman steering, the radius of the outer wheels is at a greater distance in the circumventing circle than that of the inner wheels, the following applies:

$$\cot \theta_i - \cot \theta_o = -\frac{d}{l}. \quad (4.4)$$

With a wheel distance of $d = 277$ mm and $l = 365$ mm, this results in the table shown in Table C.1.

Hardware Selection

For the drive of the wheels, BLDC motors were chosen. In contrast to stepper motors, these are optimised for a uniform torque and not for precise motion control. The resulting torque of each wheel can be calculated to:

$$\tau = R_{\text{total}} \cdot \left(\frac{d_w}{2} - \delta \right). \quad (4.5)$$

The required power is then resulting in:

$$P = \tau \cdot \left(\frac{2v_{\max}}{d_w} \right), \quad (4.6)$$

with the estimated maximum velocity v_{\max} .

4.2.3 Deployment mechanism

4.3 Electrical Power System

The EPS (Electrical Power System) is the subsystem responsible for the electrical power supply of INSPIRE. It consists of four fundamental parts, which are the energy source, the PCDU unit (Power Control and Distribution) and the Energy Storage as well as the rover subsystems as the consumers. The EPS is visualized in Figure 4.3.

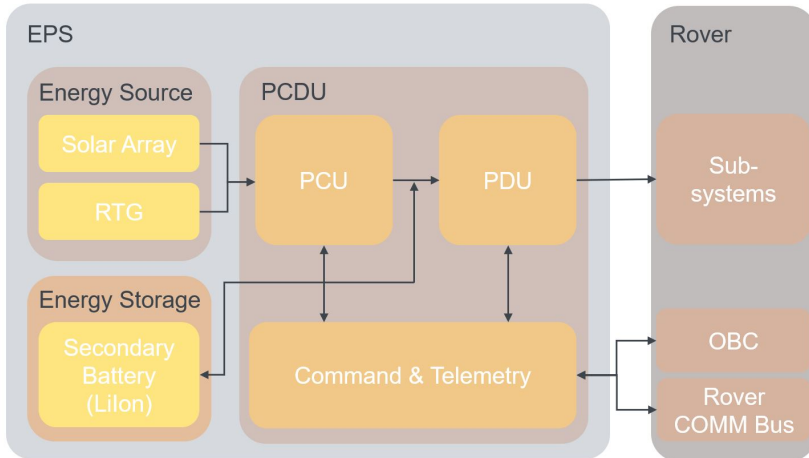


Figure 4.3: Functional Flow Chart Diagram for the EPS Subsystem.

4.3.1 EPS Budget and Overview

Figure 4.4 summarizes the power budget of INSPIRE based on the rover system modes defined in Section 3.2. The holistic power budget can be found in Figure D.1. As can be seen, the Locomotion mode has the highest demands on the EPS. The two payload modes also have a high power demand. The Communication mode also has a high consumption. However, since this is primarily used at night and the rover can be charged again afterwards without any problems, it does not place any major restrictions on the power budget. Idle/Perception mode has a low consumption, but is usually used for a long time at a stretch and therefore also places high demands on the EPS. In Charging mode, the EPS is able to charge $8.82 W_{el}$.

4.3. ELECTRICAL POWER SYSTEM

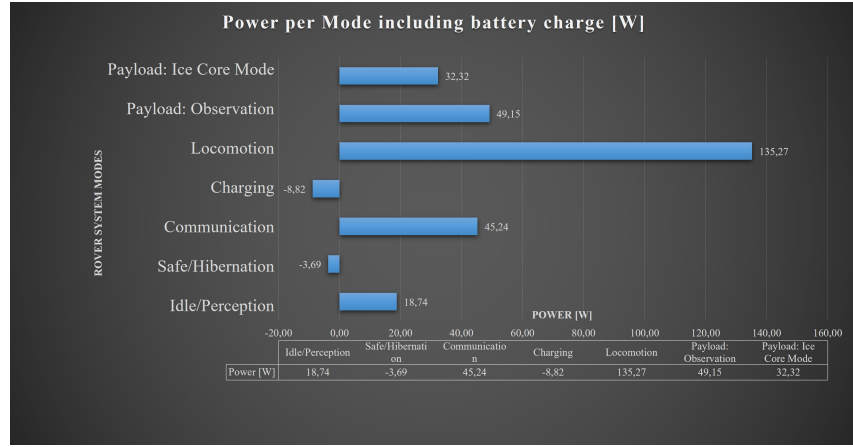


Figure 4.4: Functional Flow Chart Diagram for the EPS Subsystem.

4.3.2 Energy Source

For the energy generation of INSPIRE many possible sources were taken into consideration for a trade-off. As a conclusion of this trade-off the decision was made to utilise a Radioisotope Thermoelectric Generator (RTG) as the main energy source for INSPIRE.

As the research couldn't find an RTG with a mass suitable for INSPIRE, the solution was to scale down a bigger RTG as an approximation. As a baseline of the scaling the eMMRTG (Enhanced Multi Mission Radioisotope Thermoelectric Generator) was utilised, which is currently under development at NASA and is especially designed for deep space missions like Europa. For the scaling a goal RTG mass of $m_{RTG} = 3 \text{ kg}$ was defined and the eMMRTG was scaled down using the given data.

In Table 4.3 the scaling results for the eSMMRTG (Enhanced and Scaled Multi Mission Radioisotope Thermoelectric Generator) are listed. The eSMMRTG has a BOL specific power of $\alpha_{BOL} = 4.0 \frac{W_{el}}{kg}$ and provides an electrical power of $P_{el} = 12.08 \text{ W}_{el}$ during the mission duration[7][8][9][10][11].

Table 4.3: Parameters for the scaled eSMMRTG based on the eMMRTG.

Scaled eSMMRTG Parameter	Unit	Value
System Mass m_{RTG}	kg	3.5
BOL Specific Power α_{BOL}	$\frac{W_{el}}{kg}$	4.0
BOL Power $P_{el,BOL}$	W_{el}	14
Isotrop	-	Pu-238
Isotrop Half-Life	a	87.7
Flight time and Storage (incl. Margins)	a	7
Power Loss Degradation until BOM	W_{el}	0.56
BOM Power $P_{el,BOM}$	W_{el}	13.44
Europa Day Duration	h	85
Mission Duration	d	106.25
End of Mission Power $P_{el,EOM}$	W_{el}	13.42
Final Power for Study P_{el} (incl. 10 % scaling Margin)	W_{el}	12.08

Furthermore INSPIRE will also be equipped with some radiation hardend solar arrays as already explained in Section 2.5[6]. Since these solar cells are primarily used for technology testing, the mission must also be able to operate completely without this generated energy. For this reason, and because the expected energy generated by the solar cells is minimal, only the energy generated by the RTG is considered for the Phase 0 Study. However, it should be noted that these solar cells will also generate a certain amount of energy, which will benefital for the EPS.

4.3.3 Energy Storage

For the energy storage of INSPIRE many possible battery types were taken into consideration for a trade-off. As a conclusion of this trad-off the decision was made to utilize LiIon batteries as the secondary batteries of INSPIRE. This decision is primarily based on LiIon batteries high energy density, temperature range, robust performance and long operating and cycle life in extreme environments[12]

As the RTG only generates a small constant power the main energy source during the mission will be the accumulated energy of the batteries. The rover will charge the batteries at night, so the next exploration day can start with full capacity. Furthermore the batteries have to be charged during day time to maintain operations.

For the sizing of the batteries, the rover motion was chosen as the design driver, since this is the highest energy consuming state of the rover and additionally mission critical for INSPIRE. The rover motion consists of an interaction of the Locomotion and Perception mode as already mentioned in Chapter 3. Therefore it was defined that INSPIRE shall be able to drive 50 m (including alternating Locomotion and Perception Mode) with a fully charged Battery. Furthermore the battery mass shall not exceed 2 kg. The required battery capacity $C_{\text{Batt},\text{req}}$ can be caculated using Equation 4.7. The results are listed in Table 4.4 [13].

$$C_{\text{Batt},\text{req}} = \frac{P_{\text{el},\text{req}} \cdot t_e}{DoD \cdot \eta_{\text{LiIon}}} \quad (4.7)$$

Table 4.4: Power consumption mode used as design case for the battery sizing.

Power Consumption Mode:	Unit	Locomotion	Perception
Required Electrical Power $P_{\text{el},\text{req}}$	W _{el}	135.27	18.74
Duration of the mode t_e	s	500	15000
DOD for Dimensioning	-	0.90	0.90
Efficiency of LiIon Cells η_{LiIon}	-	0.95	0.95
Required Battery Capacity per mode C_{mode}	Wh	21.97	91.33
Total Required Battery Capacity $C_{\text{Batt},\text{req}}$	Wh	113.30	

Using these values a suitable battery cell and battery design configuration were conducted. Under consideration of these parameters the battery capacity C_{Batt} can be calcuated:

$$C_{\text{Batt}} = C_{\text{cell}} \cdot V_{\text{cell}} \cdot N \cdot M. \quad (4.8)$$

According to the ECSS reliability restrictions 1 battery string must be substracted for dimensionsing. Furthermore a 30 % margin on the energy content was applied. This leads to a final battery configuration with a capacity of $C_{\text{Batt}} = 156.24$ Wh and a mass of $m_{\text{Batt}} = 1980$ g. The final battery values are listed in Table D.1 [14].

4.3.4 EPS Power Control and Distribution

In order to ensure the full functionality of the EPS, the last main component to be selected is a suitable PCDU. As described in Figure 4.3, the PCDU forms the heart of the EPS and is an important interface to the OBC and COMM. Furthermore the PCDU shall be able to monitor and control the rover system if necessary through watchdogs, HPC (High Priority Commands) and direct connections to the OBC and COMM.

The PCDU has the challenging task not only to process the RTG as the main energy source, but also to process solar cells as secondary energy sources. Therefore, a PCDU was sought which has the required size, dimensions and range of functions. The research resulted in the Nova PCDU from Bradford DSI. In addition, margins were added to the PCDU to ensure feasibility[15].

4.4 Communications and Command & Data-Handling

The Communications subsystem consists of redundant transmitters and receivers which are cross strapped to four antennas and the OBC. Additionally hard wired connections linking the communication system to the PCDU enable for reboots via direct commands.

C&DH is responsible for the generation of telemetry from the housekeeping boards and the execution of telecommands, as well as the storing and compressing of payload data.

4.4.1 Operational Concept

Due to power and time constraints, the rover will transmit only telemetry during the locomotion and payload campaigns. Payload data will be compressed, stored and forwarded to the Lander at the end of a mission day.

To achieve the scientific output from Section 3.1 the transmission time per european day is calculated in Subsection E.2 (Table E.4) and adds up to 38,23 minutes.

4.4.2 Communication System

Requiring too many resources a direct link to earth has been deemed impractical. Instead communication for the INSPIRE mission is proposed to rely on a link between the rover and the Europa Lander. The lander then forwards data to earth via a satellite relay carrier which orbits the moon. The lander offers a 25 dB high gain antenna [Missing Reference] and a low gain antenna which is not further specified in literature.

The downlink from the rover to the lander has been identified as the critical transmission path. However, link budget considerations in Subsection E.1 reveal that a transmission to the LGA of the Europa Lander produces a link margin of 10,59 dB, resulting in a Bit Error Rate of less than 10^{-4} . The link budget has been performed under the conservative considerations listed in Table E.1.

Using the Landers LGA greatly increases robustness due to the elimination of pointing errors and higher margin for rover positioning error. Additionally, the INSPIRE rover's communication link would not interfere with the Landers communication to the relay carrier by blocking the HGA.

Component Selection

Due to the considerably high link margin the focus is on low mass and low power components with flight heritage such as flown on CubeSat missions. Criteria with relatively small impact on

the link budget such as component noise or even FEC have not been taken into account. The rover communication uses X-Band for increased compatibility with the lander and has a total system mass of less than 1 kg.

Since radiation hardness was not included in most data sheets a total dose of < 20 krad was assumed in accordance with values for LEO [Missing Reference].

The selected components are listed in Table 4.5.

Table 4.5: Key criteria of selected communication components

Component	Supplier	Part Description	1. Criteria	Value	2. Criteria	Value
Transmitter	Sputnix	SXC-XTX-01	mass	0,195 kg	data rate	10 Mbit/s
Receiver	Endurosat	S-Band receiver	power	max. 2 W	mass	0,220 kg
Antenna	Endurosat	patch antenna	mass	2,2 g	frequency	X-Band

Expected transmission times per mission day are less than 40 minutes (see Subsection E.2, Table E.4). Therefore the transmitter mass is identified as more critical than power.

Receiver duty cycles on the other hand range close to 100 % (REFERENCE POWER BUDGET). Thus power has been identified as the most crucial criteria.

A passive X-Band antenna was selected due to compact dimensions and zero power consumption. The entire trade off can be found in (APP Trade off).

4.4.3 Command & Data Handling

With respect to restricted power supply a redundant OBC hot-cold configuration stands to reason. Additionally, the standby mode is suggested during hibernation and charging modes relying solely on the PCDU (see chapter [Missing Reference]). Emphasis for the Electronics selection is placed on flight proven radiation hardness to increase mission robustness in the high radiation environment of the Jupiter system. Criteria of less importance are CPU speed and dimensions.

Instead of designing a new OBC board a trade-off was performed among existing single board computers. SBCs provide peripheral services such as bus interfaces, timer and memory in a flight proven configuration, which promises an effective mission development.

BAE Systems provides a SBC with their flight proven Power PC750 Architecture which withstands a total radiation dose of up to 1 Mrad. The robustness comes at the cost of a 182 MHz processor speed (DATASHEET REFERENCE).

Additionally a custom housekeeping board will be tasked with providing engine control peripherals and sensor read out electronics.

4.5 Thermal Control System

The main object of the Thermal Control System (TCS) is to keep the eletric components within their temperature limits, listed in Table F.8. As a result of Europas low surface temperature, a small solar constant and the thin atmosphere the heat loss of the rover has to be minimised [16]. This shall be reached by a smart heat distribution as well as by an adequate insulation and surface finishing.

4.5.1 Concepts

The main heat source of the rover is the waste heat of the RTG (see Section 4.3), which will be lead by thermal straps to the thermperature sensetive components. Carbon-based straps *LyNX®* with a high thermal conductivity to density ratio will be used, [17]. However, the thermal conductivity is highly depend on the materials temperature, see Figure 4.5. The curve was approximated by an cubic interpolation, Figure F.3 and Equation 5.14. To consider heat loss as a result of surface contact and radiation, the thermal conductivity was reduced about 20 % ($f_r = 0.8$).

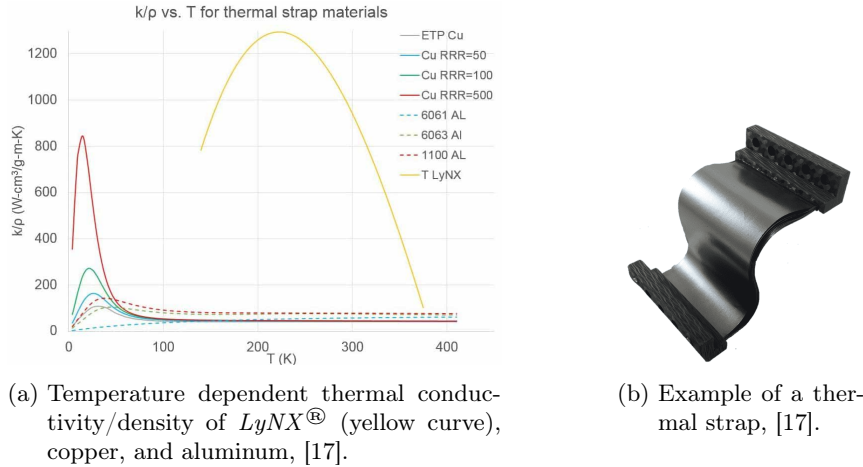


Figure 4.5: Carbon-based thermal strap *LyNX®*.

The camera, exposed on a mast, will be heated by a seperate, light weight Radioisotope Heater Unit (RHU), which has been used during several NASA missions [18]. For the insulation, the material *Aerogel* will be applied, which has a very low heat conductivity ($0.016 - 0.03 \frac{W}{mK}$) as well as a low density ($5 - 200 \frac{kg}{m^3}$) and has also been used in space applications [19].

To avoid the risk of overheating, concerning the ebay, camera and drive engine, special bi-metallic heat switches (see Figure 4.6) will be placed between the application and the connection interface. These switches change their heat conductivity beyond a certain temperatur due to the expansion of the disk (see Figure 4.7a). It was assumed, that the toggle temperatur can be adapted by increasing the disk height. The influence of the changed disk stiffens on the contact pressure and therefore the heat conductivity was neglected for this study. The measured heat conductivity characterisitc was divided in three linear sections (Figure 4.7b), to enable a simple modelling in the upcoming thermal calculation. For the most componets, a cost-efficient sand blasting of the surface is applicable. For special requirements, white paint will be used, Table F.12.

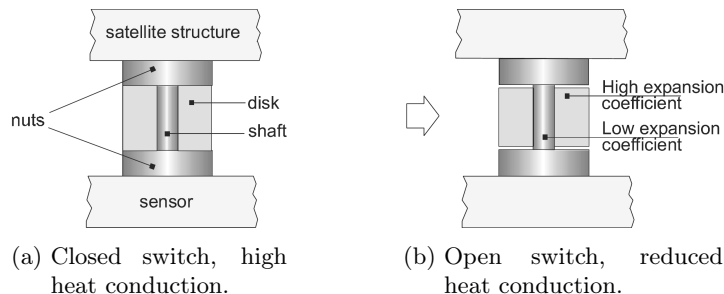


Figure 4.6: Bi-metallic heat switch, [20].

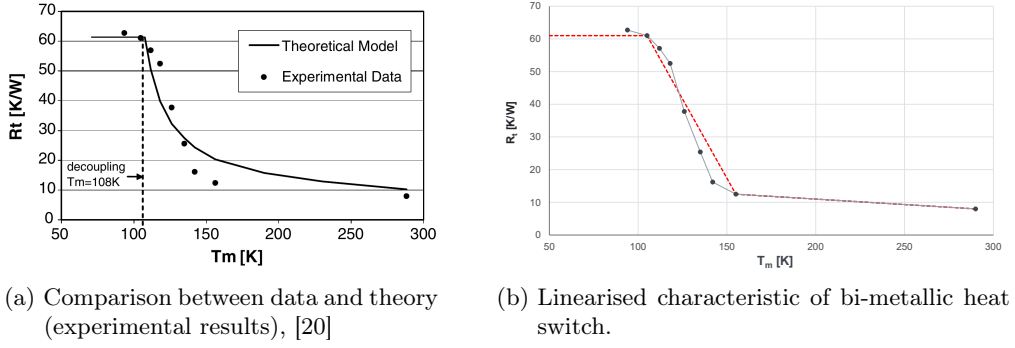


Figure 4.7: Change of the heat switch conductivity R_t over the mean temperature T_M .

4.5.2 Thermal Network

A thermal analysis was performed in order to get

- the dimension of the insulation and heat straps,
- the necessary amount of RHUs and heat switches,
- the required surface finishing and
- the suitable choice of material.

For that, a thermal network with ten nodes was derived from the rover, shown in Figure 4.8. At the intersection of the steering and drive engine, two additional nodes were defined to calculate the heat flow.

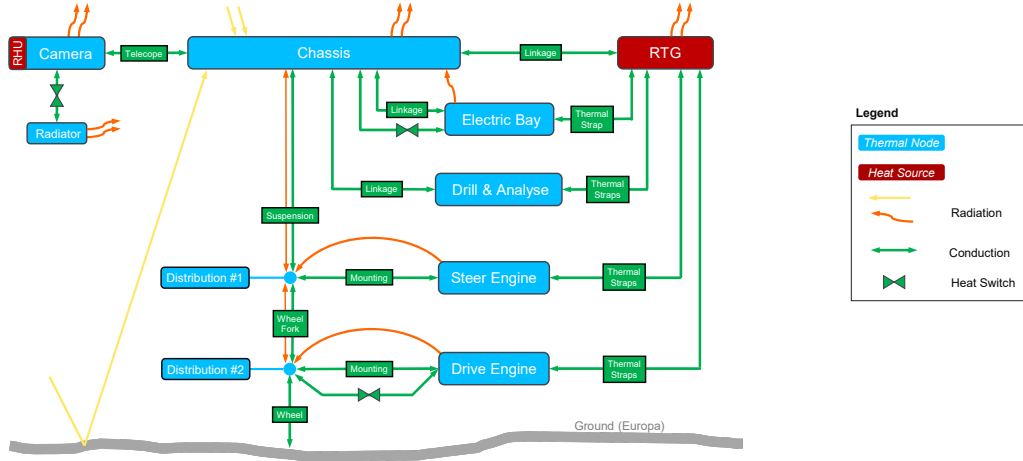


Figure 4.8: Thermal network of the rover.

On the basis of the thermal network, the heat energy equilibrium for each node was defined (see Subsection F.1). The calculation were considered as a quasi-static analysis, were the component temperatures stay constant, $\frac{dT}{dt} = 0$. Due to the early state of the rover, simplifications and assumptions for the analysis were made.

- The convection was neglected due to the thin atmosphere.
- The whole electrical power of the components will be dissipated into heat.

- A variation of $\pm 20\%$ for the emissivity and absorptivity values was considered, if applicable (see Table F.10).
- The heat as a result of retardation radiation inside the shielding was neglected.
- No discrete nodes for the radar, hazcams, APXS and deployment engines were considered. Their heat will be lead into the chassis.
- The mechanism engines weren't considered.
- A half of bogies radiation loss were put to the chassis and Node 1 each.
- A half of wheel forks radiation loss were put to the Node 1 and Node 2 each.
- No discrete nodes for the radar, hazcams and deployment engines were considered. Their heat will be lead into the chassis.

4.5.3 Analysis

The thermal analysis was performed as an Excel calculation with the possibility to adapt input values and dimension.. The major driving load cases are the hot and the cold cases, where the maximum and minimum temperatures of the rover components will be reached. For that, the most powerful components were set to operating mode at once or only the minimum required components were turned on, respectively. The emissivity and absorptivity were adjusted to fulfil the cases. There were further load cases defined to consider the battery charging, the communication mode and the drill & analyse operation.

4.5.4 Results

The resulting temperatures for each node for the hot and cold cases are listed in ???. The temperature margins for uncertainties, acceptance tests and qualification tests were considered with 5 K each, ± 15 K in total, [21]. The corresponding temperatures are listed in Table 4.6. All temperature lay between their limits without using a heater. Considering the temperature margin, the electric ebay exceeds the temperature limits of the transmitter, Table 4.7. The issue can be solved by optimising the heat paths and adding further insulation during the detailed E-Bay design process. Yet another results can be found in Table F.1 to Table F.5, Table F.7 and Table F.9.

The thermal analysis was performed as an Excel calculation, which can be found in the corresponding folder of Team 3. The calculation sheet offers the possibility to adapt and customise input values and dimension. The major driving load cases are the hot and the cold cases, where the maximum and minimum temperatures of the rover components will be reached. For that, the most powerful components were set to operating mode at once or only the minimum required components were turned on, respectively. The emissivity and absorptivity were adjusted to fulfil the cases. There were further load cases defined in order to cover important mission cases.

4.5.5 Results

The resulting temperatures for each node for the hot and cold cases are listed in ???. The temperature margins for uncertainties, acceptance tests and qualification tests were considered with 5 K each, ± 15 K in total. The corresponding temperatures are listed in ???. All temperature lay between their limits without using a heater. Nevertheless, heaters were considered for the power calculation, see Section 4.3.

In a further step, a more detailed analysis should to be carried out with the Finite-Element-Method to identify the correct heat and temperature distribution. The FE results could be used

Table 4.6: Temperature results in K of thermal analysis, *with out* margin .

Components	Hot Case	Cold Case	Charging	Communication	Analyse
RTG					
Electric Bay					
Drill & Analyser					
Camera					
Steering Engine					
Drive Engine					

Table 4.7: Temperature results in K of thermal analysis, *with ±15 K* margin .

Components	Hot Case	Cold Case	Charging	Communication	Analyse
RTG					
Electric Bay					
Drill & Analyser					
Camera					
Steering Engine					
Drive Engine					

to verify and adjust the analytical analysis to get a helpful tool for fast thermal calculation to evaluate different materials or designs in the further development phases.

4.6 Radiation

Compared to the radiation environment near Earth the radiation environment near Jupiter is multiple times stronger. It has the highest radiation levels of any planet in our solar systems [Platzhalter]. In order to survive these harsh environmental conditions, special emphasis must be placed on the radiation protection. In Figure G.1, the average trapped proton and electron fluxes on Europa's orbit around Jupiter are shown in comparison to the outer Van Allen radiation belt around Earth. However, in contrast to the Van Allen radiation belt, the duration within the radiation environment on Europa cannot be minimised and the rover has to be designed to withstand the entire mission duration of 30 days.

In oder to design and evaluate different radiation protection approaches, different calculations have to be performed. For this purpose the ESA SPace ENVironment Information System (SPENVIS) is used [Platzhalter]. All calculations and figures in Section 4.6 are performed with SPENVIS unless otherwise stated.

4.6.1 Radiation Protection

Various options are available to protect the rover against the radiation. A common approach is the use of aluminium or titanium as these materials can also act as structural elements. However, due to the mass constraints of 30 kg other materials or material compositions are taken in consideration which are more mass effective. In Table 4.8, an optimised shield structure is presented for different weight thresholds designed for the radiation environment around Jupiter.

The difference between an aluminium or titanium shielding and an optimised structure listed in Table 4.8 for the total ionizing dose (TID) is shown in Figure G.2.

Due to the mass savings of the optimised structure it will be used where the radiation protection of the aluminium structure is not sufficient. In order to reduce the mass further, a radiation vault is utilised that highly sensible components do not have to be shielded separately.

Table 4.8: Optimal shield structure for an Jupiter mission. [Platzhalter]

Areal Density / g/cm ²	0.5	1	2	3
Layer No. 1 / mm	Pb 0.415	Pb 0.829	W 0.984	Ta 1.563
Layer No. 2 / mm	Fe 0.033	Mg 0.158	Mg 0.540	Al 0.399
Layer No. 3 / mm	-	-	-	Mg 0.150

4.6.2 Components

Every component on the rover has a different radiation tolerance and therefore have to be placed at different compartments within the rover. The radiation tolerances are listed in Table G.1. None sensitive components like the electric motors and harness are only shielded by an aluminium structure where components like the metal within the wire are resistant against the radiation. However, isolators around the cables have to be selected to be resistant in order to prevent short circuits. Highly sensitive components like cameras have an additional protective layer in order to reduce the TID to under 30 krad. Components which are within the rover like the on-board computer (OBC) are placed within the radiation vault which reduces the TID to under 20 krad. For this purpose the optimised shield structure with a weight target of 0.5 g/cm² is used. Detailed TIDs for all components are shown in Figure G.3.

4.6.3 Improvements

Even though the radiation protection is sufficient for the rover to survive at least the nominal mission of 30 days, further improvements can be performed in order to extend the secondary mission.

Local shielding can be applied on less resistant components in order to reduce the wall thickness of the whole radiation wall. If components with a radiation tolerance under 43.27 krad are individually shielded a mass saving of 736.2 g can be achieved. Additionally, water ice extracted from the surface of Europa can be used to improve the radiation protection. With a layer of one centimetre of water, the TID within the radiation vault can be reduced to 16.03 krad without the additional radiation protection beside the 4 mm of aluminium structure. The start mass of the rover can therefore be reduced by 897.2 g by removing the additional shielding.

Detailed calculations for local shielding and water improvements can be found in Appendix G.3 and may be analysed further in Phase B.

4.6.4 Conclusion

In order to protect the rover against the high radiation levels at the surface of Europa, the rover has different compartments. High sensible components are placed within a radiation vault which has a mass optimised structure. Components which has to be outside the radiation vault but are highly sensible are shielded individually. Low sensible Components are protected by the

Aluminium structure. Figure 4.9 illustrates the different compartments within the rover and the accorded TIDs.

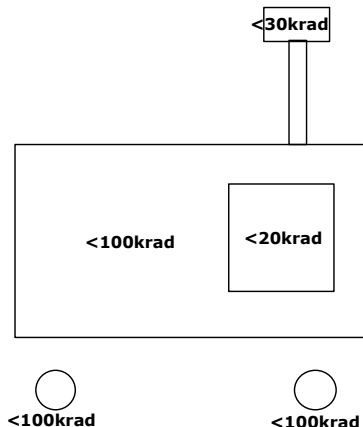


Figure 4.9: Overview of TIDs within different compartments within the rover.

Chapter 5

Outlook & Risk Assessment

5.1 Risk Assessment

To reduce risks and increase the robustness within the development process for the INSPIRE mission, all subsystems focus on flight proven or space grade hard ware. Table 5.1 provides an overview on the resulting TRL for each subsystem.

Subsystem	overall TRL	Deviating component
Payload	0	Drill System and Sample Analyser TRL 0
Structure & Mechan.	9	Boom Mechanism TRL 0
Locomotion	9	none
EPS	9	PCDU may be customized
TCS	9	none
COMs, C&DH	9	Housekeeping TRL 0

Table 5.1: Subsystem TRL for risk assessment

Housekeeping electronics and the Boom Mechanism to extend the camera head for the INSPIRE mission will be custom designed components and therefore rated at TRL 0. However due to proven development processes and simple testing the risk for the mission progress is rated non critical.

Payload components development depict the highest risk for the mission. The Analyser for the ice core samples is a downsized replica of the [missing reference]. The ice core drill derives from the Nano Drill offered by Honeybee Robotics [Missing reference]. Although the technology is available, the drill has to be adapted and tested. Testing in analog conditions potentially takes place in the arctic region and therefore lengthen the mission development process.

As a conclusion the payload subsystem development contains the highest risk for the INSPIRE mission. However the risk is considered manageable. Additionally investing in payload development is regarded worth the risk taking as it is integral to the successful investigation of Europa.

5.2 Outlook

For the TCS, a more detailed analysis should to be carried out with the Finite-Element-Method to calculate the local heat and temperature distribution. The FE results could be used to verify and adjust the analytical analysis to get a helpful tool for fast thermal calculation to evaluate different materials or desings in the further development phases.

Bibliography

- [1] Jet Propulsion Laboratory. *Galileo Mission to Jupiter*. [online] \url{https://www.jpl.nasa.gov/missions/galileo}.
- [2] NASA Science. *Europa Ocean Moon*. [online] \url{https://solarsystem.nasa.gov/moons/jupiter-moons/europa/in-depth/}.
- [3] Institut für Planetenforschung, DLR. *Die Mission JUICE zum Jupitersystem*. [online] \url{https://www.dlr.de/pf/desktopdefault.aspx/tabid-10617/18438_read-43016/}.
- [4] NASA. *Europa Lander*. [online] \url{https://europa.nasa.gov/}.
- [5] NASA / JPL. *Europa*. [online] \url{https://www.jpl.nasa.gov/missions/europa-lander}.
- [6] Fraunhofer Institute for Solar Energy Systems ISE. *RadHard Project Website*. 2021. [online] \url{https://radhard.org/}.
- [7] R. Abelson et al. *Enabling Exploration with Small Radioisotope Power Systems*. Ed. by NASA JPL. 2004.
- [8] S. Magdum. *Model Based Development of The Enhanced Multi-Mission Radioisotope Thermoelectric Generator and Effect of Thermoelectric Element Length on eMMRTG*. Ed. by Western Michigan University. 2019. [online] \url{http://homepages.wmich.edu/~leehs/ME539/Final%20Presentation%20on%20eMMRTG.pdf}.
- [9] Holgate, T. C.; Bennett, R.; Hammel, T.; Caillat, T.; Keyser, S., and Sievers, B. “Increasing the Efficiency of the Multi-mission Radioisotope Thermoelectric Generator”. In: *Journal of Electronic Materials* 44.6 (2015), pp. 1814–1821. ISSN: 0361-5235. DOI: \url{10.1007/s11664-014-3564-9}.
- [10] JPL NASA. *Enhanced Multi-Mission Radioisotope Thermoelectric Generator (eMMRTG) Concept*. Ed. by NASA JPL. 2014. [online] \url{https://rps.nasa.gov/resources/56/enhanced-multi-mission-radioisotope-thermoelectric-generator-emmrtg-concept/}.
- [11] Lakdawalla, E. *The Design and Engineering of Curiosity*. Cham: Springer International Publishing, 2018. ISBN: 978-3-319-68144-3. DOI: \url{10.1007/978-3-319-68146-7}.
- [12] S. Fasoulas et al. *Lecture Series: Energy Systems for Space Application SS 2020*. 2020.
- [13] S. Klinkner; P. Winterhalder, and M.Nitz et al. *Lecture Series - Rover System Technology SS2021*. 2021.
- [14] SAFT Batteries. *Datasheet - SAFT MP 176065 xlr*. 2018. [online] \url{https://www.saftbatteries.com/products-solutions/products/mp-small-v1}.
- [15] Bradford Space. *Datasheet - Nova PCDU*. Ed. by BRADFORD ENGINEERING BV. 2019. [online] \url{https://satsearch.co/products/bradford-nova-pcdu}.
- [16] “The surface temperature of Europa”. In: *Heliyon* 5.6 (2019), e01908. ISSN: 2405-8440. DOI: \url{https://doi.org/10.1016/j.heliyon.2019.e01908}.
- [17] Thermal Space and Thermal Straps. *Graphene Thermal LyNX® Technology*. [online] \url{https://thermal-space.com/thermal-lynx/}.
- [18] NASA. *Light-Weight Radioisotope Heater Unit*. [online] \url{https://rps.nasa.gov/power-and-thermal-systems/thermal-systems/light-weight-radioisotope-heater-unit/}.

- [19] NASA / JPL. *Aerogel*. [online] \url{https://solarsystem.nasa.gov/stardust/aerogel_factsheet.pdf}.
- [20] Milanze, F. H. and Mantelli, M. B. "Theoretical and experimental studies of a bi-metallic heat switch for space applications ". In: *International Journal of Heat and Mass Transfer* 46.24 (2003), pp. 4573–4586. ISSN: 0017-9310. DOI: [https://doi.org/10.1016/S0017-9310\(03\)00294-1](https://doi.org/10.1016/S0017-9310(03)00294-1).
- [21] S. Klinkner date = 2020, t. T. i. I.
- [22] Aluminium Giesserei Hannover GmbH. *Produktdatenblatt AA5083*. [online] https://www.leichtmetall.eu/site/assets/files/datenblatt/5083_Produktdatenblatt_A4.pdf.
- [23] Aluminium Giesserei Hannover GmbH. *Produktdatenblatt AA6082*. [online] https://www.leichtmetall.eu/site/assets/files/datenblatt/6082_Produktdatenblatt_A4.pdf.
- [24] Aluminium Giesserei Hannover GmbH. *Produktdatenblatt AA7075*. [online] https://www.leichtmetall.eu/site/assets/files/datenblatt/7075_Produktdatenblatt_A4.pdf.
- [25] Deutsche Edelstahlwerke. *1.4418X4 - CrNiMo16-5-1*. [online] \url{https://www.dew-stahl.com/fileadmin/files/dew-stahl.com/documents/Publikationen/Werkstoffdatenblaetter/Luft_Raumfahrt/1.4418_de.pdf}.
- [26] Deutsche Edelstahlwerke. *Firmodur 7225*. [online] \url{https://www.dew-stahl.com/fileadmin/files/dew-stahl.com/documents/Publikationen/Werkstoffdatenblaetter/Baustahl/1.7225_1.7227_de.pdf}.
- [27] thyssenkrupp Material Schweiz. *Titan 6Al4V "ELI"*. [online] \url{https://d2zo35mdb530wx.cloudfront.net/_binary/UCPthyssenkruppBAMXSchweiz/de/downloads/werkstoffdatenblaetter-titan/link-titan_grade_5_elis.pdf}.
- [28] thyssenkrupp Material Schweiz. *Titan Grade 5*. [online] \url{https://d2zo35mdb530wx.cloudfront.net/_binary/UCPthyssenkruppBAMXSchweiz/de/downloads/werkstoffdatenblaetter-titan/link-titan_grade_5.pdf}.

Appendix

A Operation

Number	Rover System Modes	Abbreviation	Definition
0	Launch/Off Mode	OFF	From Launch until EDL Phase Rover System is OFF Exact mode description t.b.d. and can be adapted to meet the lander demands Health tests on Occasion during flight time are foreseen (PCDU could be active) Batteries or Storage Capacity at launch and may be recharged on occasion (like Rosetta Mission) Telemetry data shall be sent by the Lander (optional if possible) RTG on => Electrical and Thermal Power may be used (for Lander Power and Thermal Systems) or is disposed of by shunts
1	Entry, Descent and Landing	EDL	From Entry until next morning after secure landing of Lander on Europa See Mode OFF PCDU ON after secure landing (Powered by RTG) Heaters ON (powered by remaining RTG Power) Battery charging if no Kill Switch is used First Morning after EDL Exact mode description t.b.d. and can be customized to lander =>Dependant on final Lander Design Critical Deployments (Egress System) and leaving the lander Optional whether Kill Switch ejected =>Battery charging can start
2	Deployment and Early Operation Mode	EOP	Rover System Activation possibilities: Kill Switch, Lander Interface, HPC from Earth PCDU ON OBC ON Heaters ON After sufficient Battery Capacity is reached (50%): Deployment of Rover Boogie and checkout/health check of all Rover Systems Afterward switching to Charging Mode
3	Idle/ Perception	ID	During Idle Operation Time Rover powered by RTG or Batteries (Excess Power charges Batteries) PCDU ON All Components in Standby or Power Saving Mode if possible Stereovision Camera ON for Orientation and Observation (Science Data) Hazcams and OBC ON for Orientation and Path Analysis COMM ON for larger time intervals (Listening Mode)
4	Safe Mode/ Hibernation (SAFE)	SAFE	Entered in case of emergency or contingency Rover Survival Mode =>Minimum Power PCDU ON COMM sends Emergency Signal then switches to COMM ON for small time intervals (Listening Mode) OBC OFF until Command received =>High Power Commands (HPC) Heaters ON Science data shall be stored without data loss Applicable during Day and Nighttime Exit after receiving the corresponding command (Optional: Timer ON and Restart of Rover System after time period has passed)
6	Communication	COMM	During Transmission of major Telemetry or Science Data Rover powered by RTG or Batteries (Excess Power charges Batteries) PCDU ON All Components in Standby or Power Saving Mode if possible OBC SB COMM ON (Transmission Mode)
7	Charging	BAT	For Battery charging Rover batteries charged by RTG PCDU ON All Components in Standby or Power Saving Mode if possible OBC SB Quit after sufficient charge is reached
8	Locomotion	LOC	For Rover Movement and Observation Locomotion and Navigation ON Hazcams and Traversing Path Analysis ON OBC ON PCDU ON COMM OFF Stereovision Camera ON for Orientation and Observation (Science Data) Only during Daytime
9	Payload Observation Mode	OBS	Payload Mode for Science Data Collection during Daytime OBC ON PCDU ON COMM OFF Stereovision Camera ON for Orientation and Observation (Science Data) RADAR ON for Ground Investigation =>Drill Location Only during Daytime
10	Payload: Ice Core Mode	ICE	Payload Mode for Science Data Collection during Daytime or Nighttime OBC ON PCDU ON COMM OFF Ice Core Drill ON during Ice Core Sample Collection Afterwards Sample will be analysed =>APXS ON

Table A.1: Collection of Rover System Modes.

B Structure and Mechanism

Table B.2: INSPIRE Mass Budget

Subsystem	Component Name	Mass per Component / kg	Quantity	Component Margin	Total / kg
Structure and Mechanism	Harness	3	1	20 %	3,60
	Chassis	look up at Chassis Table	1	20 %	5,01
	E-Bay Box	1,033	1	20 %	1,24
	Boom	0,17	1	20 %	0,20
	Solar Cell Plate	0,121	1	20 %	0,15
Locomotion	wheels	0,158	4	20 %	0,76
	rims	0,162	4	20 %	0,78
	motor (wheels)	0,057	4	10 %	0,25
	planetary gear(wheels)	0,118	4	10 %	0,52
	Motor (steering)	0,07	4	5 %	0,29
	Motor (deployment)	0,07	6	5 %	0,44
	IMU	0,012	4	10 %	0,05
EPS	Battery	1,98	1	10 %	2,18
	RTG	3,5	1	10 %	3,85
	SolarCells	0,0012975	10	20 %	0,02
	PCDU	0,33	1	20 %	0,40
COM	LGAs	0,002	4	5 %	0,01
	Transmitter	0,195	2	5 %	0,41
	Receiver	0,22	2	10 %	0,48
	Multiplexer	0,065	2	5 %	0,14
C&DH / sensors	Sun Sensors	0,016	4	5 %	0,07
	OBC	0,35	2	5 %	0,74
	temperature Sensor	0,0002	20	20 %	0,00
	Housekeeping	0,2	1	5 %	0,21
TCS	Heaters	0,00181	10	5 %	0,02
	isolation	0,15	1	20 %	0,18
	Carbon Straps	0,53	1	5 %	0,56
	RHU	0,1	1	5 %	0,11
	Magnetic Switch	0,06	6	10 %	0,40
Payload	Ice Core Drill Motor & Electronics	1,3	1	20 %	1,56
	Ice Core Drill Titanium bit	0,041	1	20 %	0,05
	Groundradar electronics	0,045	1	5 %	0,05
	Ground Radar antenna	0,00273	2	10 %	0,01
	APXS Analyzer	0,43	1	20 %	0,52
	Haz Cams	0,064	3	5 %	0,20
	Stereo Vision Cam	0,064	2	5 %	0,13
	objective StereoCam	0,08	2	20 %	0,19
	objective HazCam	0,048	3	20 %	0,17
	LEDs	0,003	16	10 %	0,05
Radiation	Cam shielding	0,02905	5	20 %	0,17
	E-Bay shielding	0,94	1	20 %	1,13
Mass with component margins and 2mm Aluminum Chassis					27,28
Mass with component margins and 1,5mm Aluminum Chassis					26,64
System Margin					10 %
Total Mass (2mm Aluminum Chassi)					30,0
Total Mass (1,5mm Aluminum Chassi)					29,31

C Locomotion

C.1 Locomotion Design Drivers

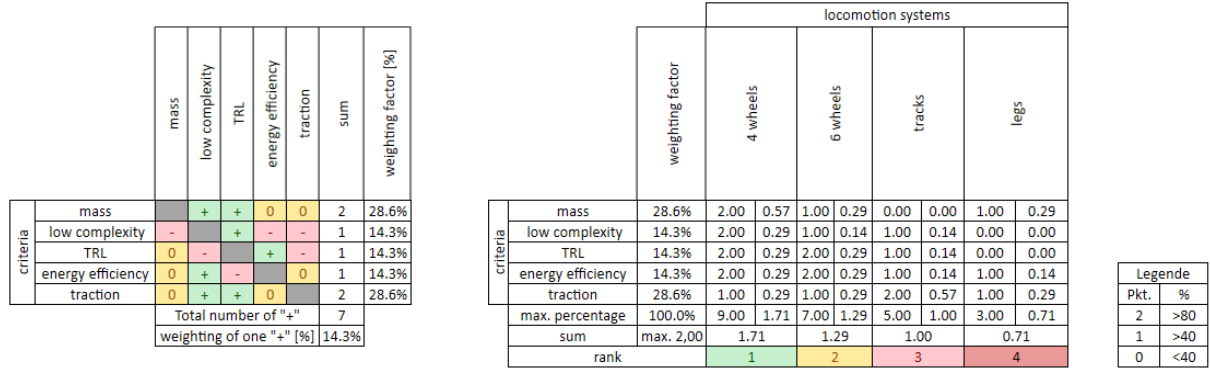


Figure C.1: Trade-off of the locomotion movement system. The criteria with the respective weighting factors are shown on the left. On the right side are the respective systems.

Terrain	Moisture Content (%)	n	k_c		k_ϕ		c		ϕ
			lb/in. ⁿ⁺¹	kN/m ⁿ⁺¹	lb/in. ⁿ⁺²	kN/m ⁿ⁺²	lb/in. ²	kPa	deg
Dry sand									
(Land Locomotion Lab., LLL)	0	1.1	0.1	0.99	3.9	1528.43	0.15	1.04	28°
Sandy loam (LLL)	15	0.7	2.3	5.27	16.8	1515.04	0.25	1.72	29°
Sandy loam (LLL)	22	0.2	7	2.56	3	43.12	0.2	1.38	38°
Sandy loam	11	0.9	11	52.53	6	1127.97	0.7	4.83	20°
Michigan (Strong, Buc hele)	23	0.4	15	11.42	27	808.96	1.4	9.65	35°
Sandy loam (Hanamoto)	26	0.3	5.3	2.79	6.8	141.11	2.0	13.79	22°
Clayey soil (Thailand)	32	0.5	0.7	0.77	1.2	51.91	0.75	5.17	11°
Heavy clay (Waterways Experiment Stn., WES)	38	0.5	12	13.19	16	692.15	0.6	4.14	13°
Lean clay (WES)	55	0.7	7	16.03	14	1262.53	0.3	2.07	10°
LET E sand (Wong)	25	0.13	45	12.70	140	1555.95	10	68.95	34°
Upland sandy loam (Wong)	40	0.11	7	1.84	10	103.27	3	20.69	6°
Rubicon sandy loam (Wong)	22	0.2	45	16.43	120	1724.69	10	68.95	20°
Grenville loam (Wong)	32	0.15	5	1.52	10	119.61	2	13.79	11°
Snow (U.S.) (Harrison)	0.79	32	102	42.2	5301	0.19	1.3	31.1°	
Snow (Sweden)	51	1.10	7.5	74.6	5.3	2080	0.48	3.3	33.7°
North Gower clayey loam (Wong)	46	0.73	16.3	41.6	24.5	2471	0.88	6.1	26.6°
Snow (U.S.) (Harrison)	24	1.01	0.008	0.06	20.9	5880	0.45	3.1	29.8°
Snow (U.S.) (Harrison)	1.6	0.07	4.37	0.08	196.72	0.15	1.03	19.7°	
Snow (Sweden)	1.6	0.04	2.49	0.10	245.90	0.09	0.62	23.2°	
Snow (Sweden)	1.44	0.3	10.55	0.05	66.08	0.87	6	20.7°	

Figure C.2: Soil Parameters

Mean Maximum Pressure

Ackerman Steering

Table C.1

Steering Angle	Mode 1	Mode 2	Mode 3
θ_o			
θ_o			

Wheel Width [m]	Wheel Diameter [m]	Weight per Wheel [g]
0.0500	0.1000	127
0.0600	0.1000	153
0.0700	0.1000	178
0.0800	0.1000	204
0.0900	0.1000	229
0.1000	0.1000	265
0.1500	0.1000	396
0.2000	0.1000	527
0.2500	0.1000	658
0.3000	0.1000	790
0.0500	0.1250	154
0.0600	0.1250	185
0.0700	0.1250	217
0.0800	0.1250	247
0.0900	0.1250	278
0.1000	0.1250	309
0.0500	0.1500	185
0.0600	0.1500	221
0.0700	0.1500	258
0.0800	0.1500	294
0.0900	0.1500	331
0.1000	0.1500	367
0.1500	0.1500	570
0.2000	0.1500	760
0.2500	0.1500	949
0.3000	0.1500	1138
0.0500	0.2000	236
0.0600	0.2000	284
0.0700	0.2000	332
0.0800	0.2000	379
0.0900	0.2000	427
0.1000	0.2000	487
0.1500	0.2000	730
0.2000	0.2000	973
0.2500	0.2000	1215
0.3000	0.2000	1458

Figure C.3: Various wheel dimensions respective to the weight. Rows highlighted in red are not considered further for system design due to the limit of 200 g weight per wheel.

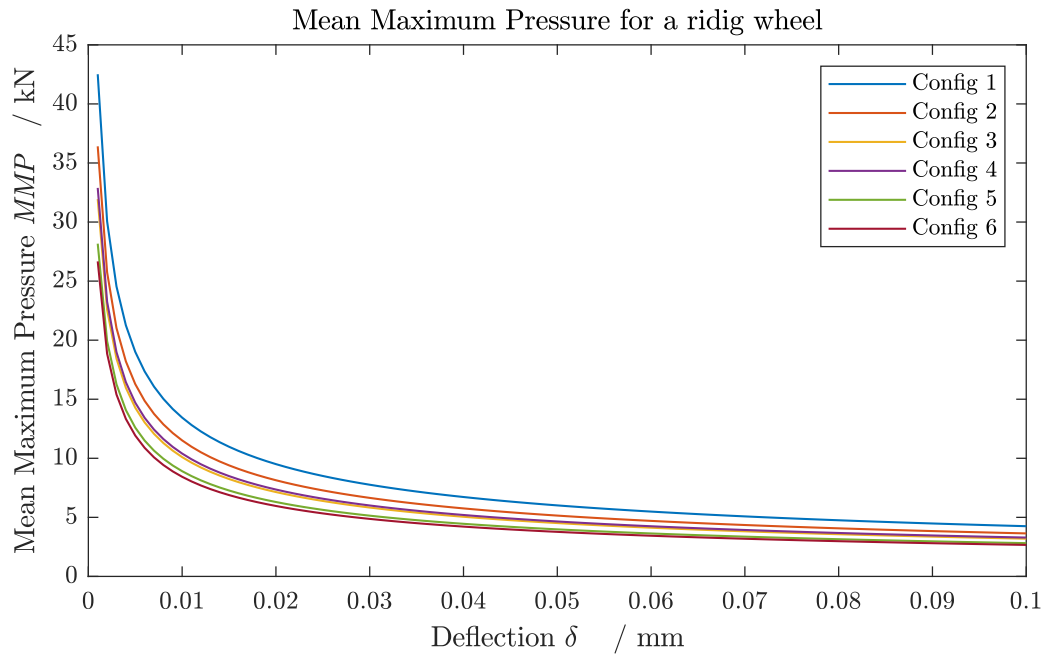


Figure C.4

Number of axles	Proportion of axles driven						
	1	3/4	2/3	3/5	½	1/3	1/4
2	3.65				4.40		
3	3.90		4.35			5.25	
4	4.10	4.44			4.95		6.05
5	4.32			4.97			
6	4.6		5.15		5.55	6.20	

Figure C.5: Parameters for the mean maximum pressure for a wheeled rover.

D Electrical Power System

Table D.1: INSPIRE battery parameters.

SAFT 176065 xlr [14]	
Configuration:	
Battery Configuration	<i>3s4p</i>
Cells in Series s N [-]	3
Cells in Parallel p M [-]	4
Cell Parameters:	
Typical Cell Capacity [Ah]	6.8
Nominal Cell Voltage [V]	3.65
Nominal Cell Capacity [Wh]	24.8
Typical Cell Mass [kg]	0.15
Energy Density [Wh/kg]	165.33
Actual Battery Configuration Parameters:	
Battery Voltage V_{Batt} [V]	10.95
Battery Nominal Capacity E_{Batt} [Wh]	297.6
Battery Mass [kg]	1.8
Battery Mass m_{Batt} (incl. 10% Margin) [kg]	1.98
Configruation according to ECSS reliability restrictions and margins included:	
Battery Configuration	<i>3s3p</i>
Cells in Series s N [-]	3
Cells in Parallel p M [-]	3
Battery Voltage V_{Batt} [V]	10.95
Battery Nominal Capacity E_{Batt} [Wh]	231.60
30% Margin on Energy Content	0.3
Battery Nominal Capacity E_{Batt} incl. Margin [Wh]	156.24
Useable Energy Density [Wh/kg]	78.91

D. ELECTRICAL POWER SYSTEM

Figure D.1: Holistic Power Budget of INPSIRE.

E Communications

E.1 Link Budget

Link budget considerations are performed under the conservative assumptions listed in Table E.1.

Parameter	Value	Unit	Symbol	Source
Rover				
antenna Gain	2	[dB]	G_R	omnidirectional LGA
output power	1	[W]	P_R	
line loss	0,6	[dB]	L_{l1}	FLP
Path				
R2L polarisation loss	0,3	[dB]	L_p	FLP
free space loss	117,55	[m^3]	L_s	
atmospheric loss	0	[dB]	L_a	negligible atmosphere
Lander				
antenna Gain	1	[dB]	G_L	conservative estimation
output power	5	[W]	P_L	conservative estimation
pointing Loss	0	[dB]	n/a	omnidirectional LGA
line Loss	0,6	[dB]	L_{l2}	FLP
eff. noise temperature	300	[K]	T_s	worst case E-bay temperature
Demodulation & Uncertain Losses				
eff. data rate	5000	[kbps]	R	50 % of max. data rate
FEC coding	none	[$-$]	n/a	
technical degradation	1	[dB]	L_{i1}	FLP
implementation loss	1	[dB]	L_{i1}	FLP

Table E.1: Transmission link parameters

The free space loss L_s [m^3] in Table E.1 is calculated using the following correlation.

$$L_s = \frac{(4\pi s)^2 \cdot c}{f} \quad (5.1)$$

The signal travel distance s is assumed to be $s = 2000 \text{ m}$ which is in excess of the mission goal described in Section 3.1. In accordance with X-Band communication the frequency f is set to a value of $f = 8,2 \text{ GHz}$. The parameter c represents the speed of light in vacuum. For simplification purposes $c = 3 \cdot 10^9 \frac{\text{m}}{\text{s}}$ is assumed.

Combining the parameters from Table E.1 the link budget is calculated using Equation 5.2. For the simplification of Equation 5.2 the line losses for the rover L_{l1} and lander L_{l2} are expressed as the sum L_l . In the same manner technical degradation and implementation losses are combined to L_i . Atmospheric losses L_a and pointing errors in Equation 5.2 are neglected due to a lack of atmosphere and the utilisation of omnidirectional low gain antennas. Parameter k describes the Boltzmann constant.

E. COMMUNICATIONS

$$\frac{E_b}{N_0} = P - L_l + G_R - 10 \cdot \log L_s - L_a + G_L + 10 \cdot \log k - 10 \cdot \log T_s - 10 \cdot \log R - L_i \quad (5.2)$$

Equation 5.2 and the conservative assumptions from Table E.1 results in an energy per bit over noise $\frac{E_b}{N_0} = 10,59 \text{ dB}$. The complete link budget can be found in Figure E.1.

Referencing Figure E.2 a Bit Error Rate of 10^{-4} can be achieved in the downlink path, which is considered sufficient for a first assessment. Optionally a FEC code can be implemented in later design phases.

Using the same parameters listed in Table E.1 leads to a $\frac{E_b}{N_0} = 50,56 \text{ dB}$ corresponding to a Bit Error Rate of potentially less than 10^{-6} . Therefore the downlink does not contribute to the design decisions. The complete link budget for the uplink path can be found in ??.

Rover Transmitter Output Power		1 Watts
		0,00 dBW
Rover total Line loss		-0,6 dB
Rover Antenna Gain	Gr	2 dBi
Rover EIRP		1,40 dBW
Downlink Path		
Rover antenna pointing loss		0 dB
R2L polarization loss		-0,3 dB
free space loss		-116,74 dB
atmospheric loss		0 dB
Signal Level at Lander	RIP	-115,64 dB
Lander		
Lander LGA pointing loss		0 dB
Lander antenna Gain	Gl	1 dBic
Signal after Lander LGA		-114,64 dB
Lander total line loss		-0,6 dB
Lander effective noise temperature		-24,77 dB
Lander signal to noise power density	C/No	88,58 dB
Data Rate		
data rate		5000 kbps
		-66,99 dBHz
Total		
System Eb/NO for Rover to Lander link		21,59 dB
Demodulation		
specified Bit Error Rate		1,00E-04 n/a
FEC coding		none
Eb/No threshold		9 dB
Uncertain Losses		
technical degradation of equipment		1 dB
implementation loss		1 dB
Total		
system Link Margin after uncertain losses		10,59 dB

Figure E.1: Rover to Lander complete downlink budget.

E.2 Mission Data Output

The analysis of the mission data concept for memory capacity and transmission times is focuses on the payload camera and Hazcams as images require far more data than telemetry or other payload data.

In a first assumption 420 images per day are stored and transmitted. Considering the sensor resolution of 2048×2048 pixels and a bit depth per pixel of 10 bit of the (CAMERA REFERENCE), a file size of 42 Mbit per image is assumed.

To calculate the message size in Table E.3, it is assumed that a transmission frame consists of 10264 bits including a payload frame of maximum 8840 bits (FLP VORELESUNG).

Table E.2: Complete link budget for Lander to Rover (L2R) transmission.

Lander to Rover (L2R) Link Budget (downlink)			
Lander			
Lander transmitter Output Power	5	W	
	6.99	dB	
Lander line loss	0.6	dB	
Lander antenna gain	1	dB	
Uplink Path			
pointing loss	0	dB	
polarization loss	0.3	dB	
path loss	116.74	dB	
atmospheric loss	0	dB	
signal level at Lander	RIP	109.65	dB
Rover			
Rover LGA pointing loss	0	dB	
Rover antenna gain	1	dB	
signal after Rover LGA	108.65	dB	
Rover total line loss	0.6	dB	
Rover effective noise temp.	24.77	dB	
Rover signal to noise power density	$\frac{C}{N_0}$	94.57	dB
Data Rate			
data rate	2	kbps	
	33.01	dBHz	
Total			
System $\frac{E_b}{N_0}$ for L2R link	61.56	dB	
Demodulation			
specified Bit Error Rate	10^{-6}	n/a	
FEC coding used	none		
$\frac{E_b}{N_0}$ threshold	9	dB	
Uncertain Losses			
technical degradation	1	dB	
implementation loss	1	dB	
Link Margin			
system link margin after uncertain losses	50.56	dB	

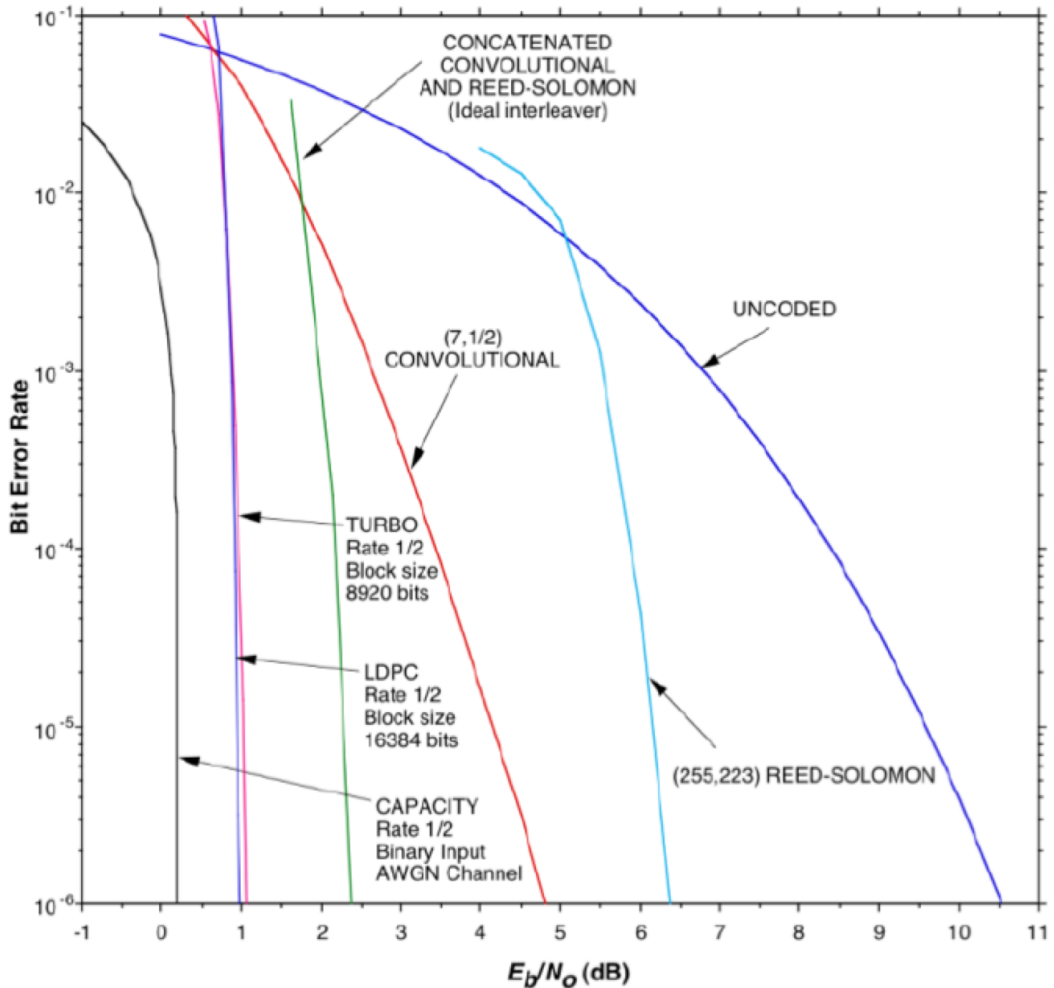


Figure E.2: Bit Error Rate for different FEC codes

The HIREW compression algorithm is suggested for the mission considering a high average compression of 0,56 % and a high compression speed of 123 Mbit/s for grayscale and 104,4 Mbit/s for RGB image files (COMPRESSSION PAPER REFERENCE).

E.3 Communications Trade Off

Transmitter Selection

Receiver Trade Off

Antenna Trade Off

E.4 Command & Data Handling Trade Off

OBC Trade Off

File Type	Compression	File Size	Message Size	Data Rate	Tx t per File
image	none	42 Mbit	48,77 Mbit	5 Mbit	8,12 s
image	HIREW	23,52 Mbit	27,31 Mbit	5 Mbit	5,45 s

Table E.3: Comparison of transmission times per image (message frame bits included)

File per tal	Compression	File Size	Total Data	Tx time
420	none	42 Mbit	2,21 GB	56,9 Min.
420	HIREW	23,52 Mbit	1,22 GB	38,23 Min.

Table E.4: Transmission time and total data output per mission day

	Mass	Power	Memory	Data Rate	RF Output Power	X-Band	CCSDS compliant	Sum	Weighting Factor [%]
Mass	+	+	+	0	+	+	+	5	27.8%
Power	-	-	+	+	+	+	+	5	27.8%
Memory	-	-	-	+	0	-	-	1	5.6%
Data Rate	0	-	+	-	-	0	1	1	5.6%
RF Output Power	-	-	-	+	-	+	-	2	11.1%
X-Band	-	-	0	+	-	-	+	2	11.1%
CCSDS compliant	-	-	+	0	+	-	-	2	11.1%
		Total "+"		18					
		Weighting "+" [%]		5.6%					

Criteria	Sputnik SXC-XTX-01	SAIT Ltd. X-Band Transmitter	GomSpace NanoCom SR2000 (Transceiver)
Mass [kg]	0.195	0.360	0.310
Power [W]	max. 15 W	max. 22	Rx 4/ Tx 4
Memory [GB]	8	None	32
Data Rate [Mbps]	max. 10	max. 5	max. 7
RF Output Power [W]	1	2.5	0.006
X-Band	yes	yes	S-Band
CCSDS compl.	No	No	Yes

(a) Weighting of selection criteria for the transmitter.

(b) Comparison of optional transmitters.

Criteria	Weighting Factor [%]	Communication			
		Sputnik SXC-XTX-01	SAIT Ltd. X-Band Transmitter	GomSpace NanoCom SR2000 (Transceiver)	
Mass	27.8%	2.00	0.56	1.00	0.28
Power	27.8%	1.00	0.28	0.00	0.00
Memory	5.6%	1.00	0.06	0.00	0.00
Data rate	5.6%	2.00	0.11	1.00	0.06
RF Ouput Power	11.1%	1.00	0.11	2.00	0.22
X-Band	11.1%	2.00	0.22	2.00	0.22
CCSDS compl.	11.1%	0.00	0.00	0.00	0.22
max. Percentage	100.1%	9.00	1.34	6.00	0.78
Sum	max. 2,00	1.34		0.78	1.22
Score		1	3		2

(c) Transmitter trade off.

Figure E.3: Transmitter Trade off for the Communication subsystem.

E. COMMUNICATIONS



Figure E.4: Receiver Trade off for the Communication subsystem.

Criteria	Mass	Cost	Gain	RF Output Power	X-Band	Sum	Weighting Factor [%]
Mass	+	+	+	0		3	42.9%
Gain	-	-	+	-		1	14.3%
RF Output Power	-	+	-	-		1	14.3%
X-Band	0	-	+	+		2	28.6%
	Total "+"					7	
	Weighting of "+" [%]					14.3%	

Criteria	Mass [kg]	0.002	Gain [dB]	max. 6	Outp Power [W]	4	X-Band	Yes	Endurosat X-Band single Patch Antenna	GomSpace NanoCom XT8250	RUAG X-Band TTC Antenna

(a) Weighting of selection criteria for the antenna.

(b) Comparison of optional antenna.

Criteria	Weighting Factor [%]	Antenna					
		Endurosat X-Band single Patch Antenna	GomSpace NanoCom XT8250	RUAG X-Band TTC Antenna			
Mass	42.9%	2.00	0.86	1.00	0.43	0.00	0.00
Gain	14.3%	1.00	0.14	2.00	0.29	1.00	0.14
RF Output Power	14.3%	2.00	0.29	1.00	0.14	0.00	0.00
X-Band	28.6%	2.00	0.57	2.00	0.57	2.00	0.57
max. Percentage	100.1%	7.00	1.86	6.00	1.43	3.00	0.72
Sum	max. 2,00	1.86		1.43		0.72	
Score		1	2	3			

(c) Antenna trade off.

Figure E.5: Antenna trade off for the Communication subsystem.

E. COMMUNICATIONS

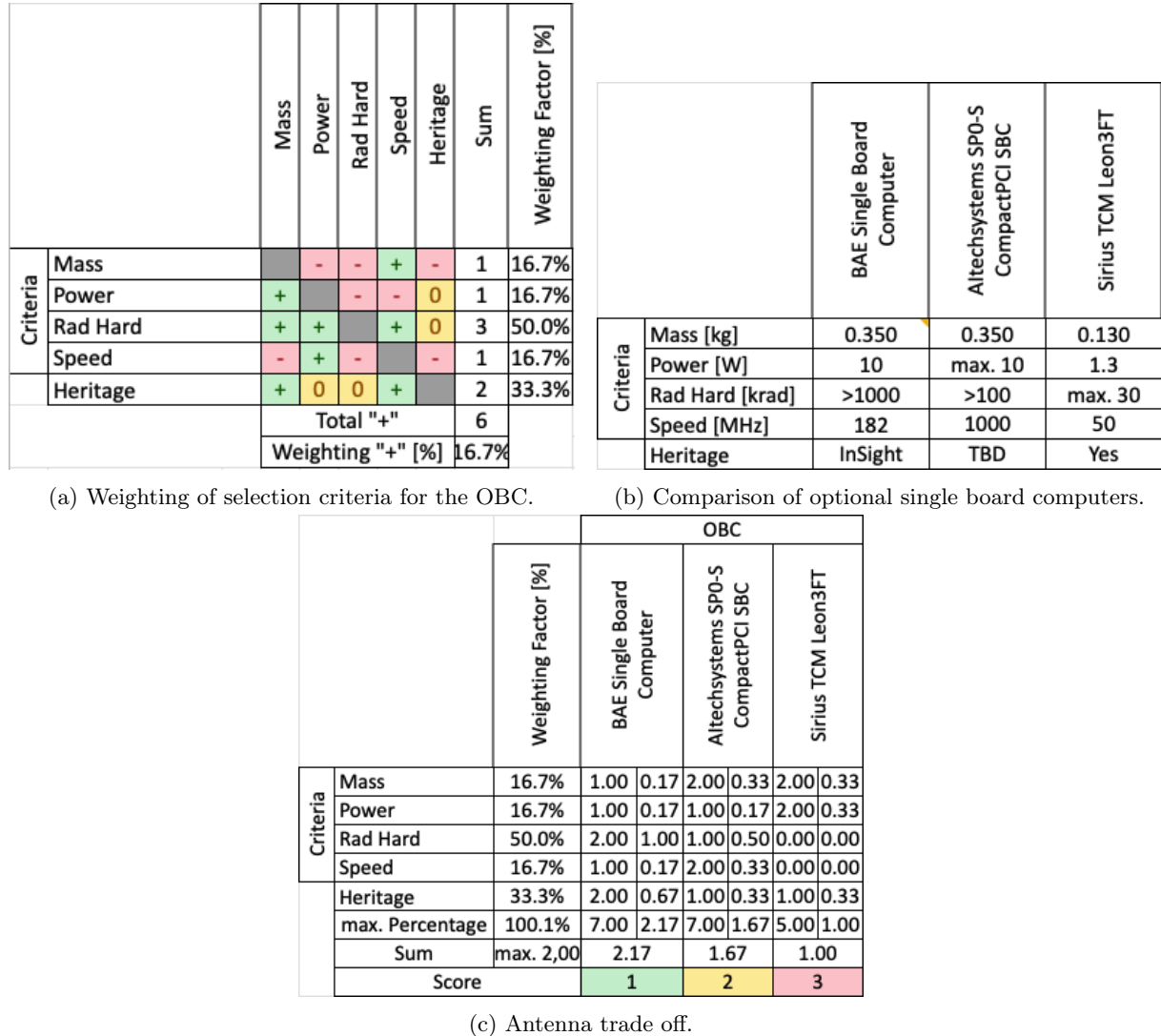


Figure E.6: OBC trade off for the Command & Data Handling subsystem.

F Thermal Controls System

F.1 Heat energy eqilibrium

The follwing equiations describe each node of the thermal network. The input values were tanken from EPS, Subsection F.2, Subsection F.3, Subsection F.4 respectively.

Subscript for eqilibrium:

Bay	Electrical Bay	Dr	Drill
Bo	Bogie	E,D	Drive Engine
Cam	Camera	E,S	Steer Engine
Ch	Chassis	WF	Wheel Fork

RTG:

$$\begin{aligned}
 0 = & \dot{Q}_{RTG} + CON_1 \cdot (T_{Bay} - T_{RTG}) + CON_2 \cdot (T_{Ch} - T_{RTG}) + \\
 & + CON_5 \cdot (T_{Dr} - T_{RTG}) + CON_9 \cdot (T_{E,S} - T_{RTG}) \\
 & + CON_{12} \cdot (T_{E,D} - T_{RTG}) - \epsilon_{RTG} \cdot \sigma_b \cdot S_{RTG} \cdot T_{RTG}^4
 \end{aligned} \tag{5.3}$$

Electric Bay: Subscript *Bay*

$$0 = \dot{Q}_{Bay} + CON_1 \cdot (T_{RTG} - T_{Bay}) + CON_3 \cdot (T_{Ch} - T_{Bay}) - \epsilon_{Bay} \cdot \sigma_b \cdot S_{Bay} \cdot T_{Bay}^4 \tag{5.4}$$

with:

$$\dot{Q}_{Bay} = \dot{Q}_{OBC} + \dot{Q}_{Tranceiver} + \dot{Q}_{Receiver} + \dot{Q}_{PCDU} \tag{5.5}$$

Drill & Analyser:

$$0 = \dot{Q}_{Dr} + CON_4 \cdot (T_{Ch} - T_{Dr}) + CON_5 \cdot (T_{RTG} - T_{Dr}) \tag{5.6}$$

Camera:

$$\begin{aligned}
 0 = & \dot{Q}_{Cam} + \dot{Q}_{RHU} + CON_6 \cdot (T_{Ch} - T_{Cam}) + \\
 & + (CON_{14} + n_{S1} \cdot CON_{S1}) \cdot (T_{Rad} - T_{Cam}) - \epsilon_{Cam} \cdot \sigma_b \cdot S_{Cam} \cdot T_{Cam}^4
 \end{aligned} \tag{5.7}$$

Radiator:

$$(CON_{14} + n_{S1} \cdot CON_{S1}) \cdot (T_{Cam} - T_{Rad}) - \epsilon_{Rad} \cdot \sigma_b \cdot S_{Rad} \cdot T_{Rad}^4 = 0 \tag{5.8}$$

Chassis:

$$\begin{aligned}
 0 = & \dot{Q}_{Radar} + \dot{Q}_{Hazcam} + CON_2 \cdot (T_{RTG} - T_{Ch}) + CON_3 \cdot (T_{Bay} - T_{Ch}) + \\
 & + CON_4 \cdot (T_{Drill} - T_{Ch}) + CON_6 \cdot (T_{Cam} - T_{Ch}) + CON_7 \cdot (T_{Node_1} - T_{Ch}) + \\
 & + \alpha_{Ch} \cdot [S_0 \cdot (1 + \rho_E) \cdot (S_{Ch1} \cdot \varphi_1 + S_{Ch2} \cdot \varphi_2) + \epsilon_E \cdot \sigma_b \cdot S_{Ch3} \cdot T_{Surface}^4] - \\
 & - \epsilon_{Ch} \cdot \sigma_b \cdot S_{Ch} \cdot T_{Ch}^4
 \end{aligned} \tag{5.9}$$

Steer Engine:

$$\begin{aligned}
 0 = & 4 \cdot [\dot{Q}_{E,S} + (CON_8 + n_{S2} \cdot CON_{S2}) \cdot (T_{Node_1} - T_{E,S}) + \\
 & + CON_9 \cdot (T_{RTG} - T_{E,S}) - \epsilon_{E,S} \cdot \sigma_b \cdot S_{E,S} \cdot T_{E,S}^4]
 \end{aligned} \tag{5.10}$$

Distribution Node 1:

$$\begin{aligned}
 0 = & 4 \cdot [CON_7 \cdot (T_{Ch} - T_{Node_1}) + CON_8 \cdot (T_{E,S} - T_{Node_1}) + \\
 & + CON_{10} \cdot (T_{Node_2} - T_{Node_1})]
 \end{aligned} \tag{5.11}$$

Drive Engine:

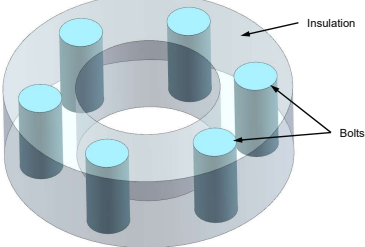
$$\begin{aligned}
 0 = & 4 \cdot [\dot{Q}_{E,D} + (CON_{11} + n_{S3} \cdot CON_{S3}) \cdot (T_{Node_2} - T_{E,D}) + \\
 & + CON_{12} \cdot (T_{RTG} - T_{E,D}) - \epsilon_{E,D} \cdot \sigma_b \cdot S_{E,D} \cdot T_{E,D}^4]
 \end{aligned} \tag{5.12}$$

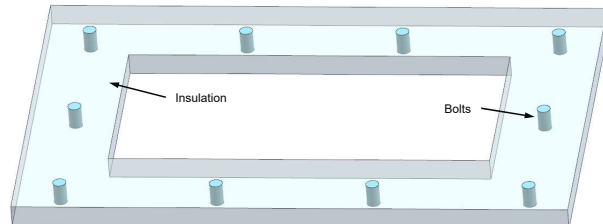
Distribution Node 2:

$$\begin{aligned}
 0 = & 4 \cdot [CON_{10} \cdot (T_{Node_1} - T_{Node_2}) + CON_{11} \cdot (T_{E,D} - T_{Node_2}) + \\
 & + CON_{13} \cdot (T_{Ground} - T_{Node_2})]
 \end{aligned} \tag{5.13}$$

F.2 Heat conductance

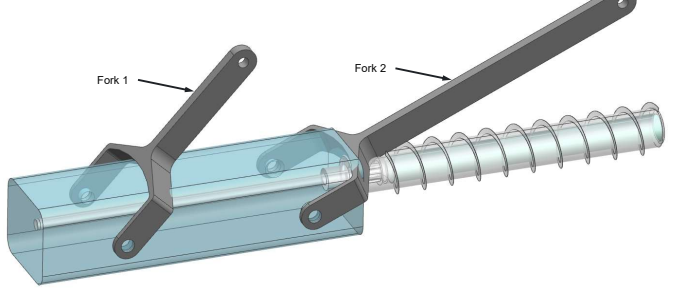
Table F.1: Definition of heat conductance C between the nodes according to Figure 4.8.

Name	Linked Components	Geometry		
Linkage	RTG \leftrightarrow Chassis			
	$CON_2 = CON_I + n_B \cdot CON_B$			
	$CON_2 = 1.50 \cdot 10^{-1} \frac{\text{W}}{\text{K}}$			
Part	Cross section	Thickness	Material	Amount
Insulation	$S_I = 3'770 \text{ mm}^2$	$t_I = 12 \text{ mm}$	Aerogel	1
Bolts, M6	$S_B = 28.3 \text{ mm}^2$	$t_B = 12 \text{ mm}$	Titan	10

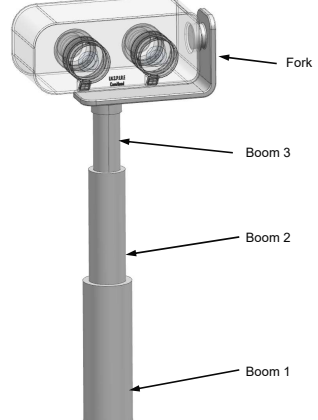
Name	Linked Components	Geometry		
Linkage	EBay \leftrightarrow Chassis			
	$CON_3 = CON_I + n_B \cdot CON_B$			
	$CON_3 = 2.80 \cdot 10^{-1} \frac{\text{W}}{\text{K}}$			
Part	Cross section	Thickness	Material	Amount
Insulation	$S_I = 27'120 \text{ mm}^2$	$t_I = 12 \text{ mm}$	Aerogel	1
Bolts, M6	$S_B = 28.3 \text{ mm}^2$	$t_B = 12 \text{ mm}$	Titan	10

F. THERMAL CONTROLS SYSTEM

Table F.2: Definition of heat conductance $CON = \frac{1}{R}$ between the nodes according to Figure 4.8.

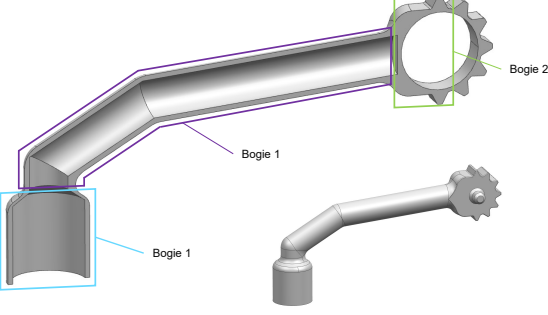
Name	Linked Components	Geometry
Linkage	Drill \leftrightarrow Chassis	

Part	Cross section	Length	Material	Amount
Fork 1	$S_{F1} = 40 \text{ mm}^2$	$l_{F1} = 90$	Aluminium	1
Fork 1	$S_{F2} = 40 \text{ mm}^2$	$l_{F2} = 150$	Aluminium	1

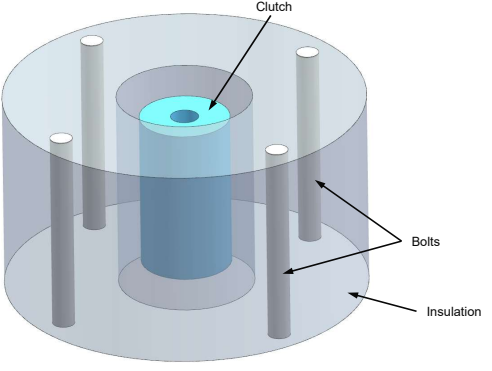
Name	Linked Components	Geometry
Telescope	Camera \leftrightarrow Chassis	

Part	Cross section	Length	Material	Amount
Boom 1	$S_{B1} = 181 \text{ mm}^2$	$l_{B1} = 116 \text{ mm}$	Aluminium	1
Boom 2	$S_{B2} = 134 \text{ mm}^2$	$l_{B2} = 95 \text{ mm}$	Aluminium	1
Boom 3	$S_{B3} = 97 \text{ mm}^2$	$l_{B3} = 60 \text{ mm}$	Aluminium	1
Fork	$S_F = 200 \text{ mm}^2$	$l_F = 170 \text{ mm}$	Aluminium	1

Table F.3: Definition of heat conductance $CON = \frac{1}{R}$ between the nodes according to Figure 4.8.

Name	Linked Components	Geometry
Suspension	Chassis \leftrightarrow Node₁	 $CON_7 = \left(\frac{1}{CON_{B1}} + \frac{1}{CON_{B2}} + \frac{1}{CON_{B3}} \right)^{-1}$ $CON_7 = 1.30 \cdot 10^{-1} \frac{\text{W}}{\text{K}}$

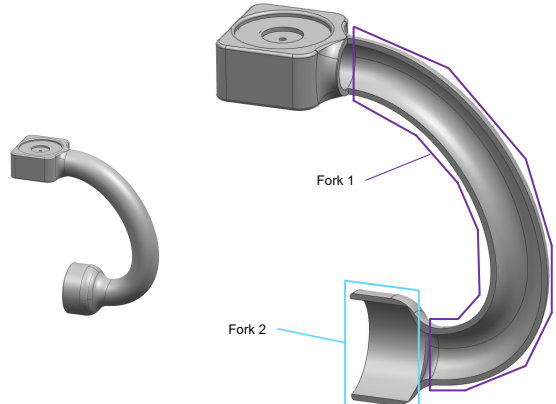
Part	Cross section	Length	Material	Amount
Bogie 1	$S_{B1} = 275 \text{ mm}^2$	$t_{B1} = 20 \text{ mm}$	Aluminium	1
Bogie 2	$S_{B2} = 113 \text{ mm}^2$	$t_{B2} = 162 \text{ mm}$	Aluminium	1
Bogie 3	$S_{B3} = 201 \text{ mm}^2$	$t_{B3} = 37 \text{ mm}$	Aluminium	1

Name	Linked Components	Geometry
Mounting	Steer Engine \leftrightarrow Node₁	 $CON_8 = CON_C + CON_I + n_B \cdot CON_B$ $CON_8 = 6.85 \cdot 10^{-1} \frac{\text{W}}{\text{K}}$

Part	Cross section	Thickness	Material	Amount
Clutch	$S_C = 45.4 \text{ mm}^2$	$t_C = 14 \text{ mm}$	Aluminium	1
Insulation	$S_I = 691 \text{ mm}^2$	$t_I = 18 \text{ mm}$	Aerogel	1
Bolts	$S_B = 3.14 \text{ mm}^2$	$t_B = 18 \text{ mm}$	Steel	4

F. THERMAL CONTROLS SYSTEM

Table F.4: Definition of heat conductance $CON = \frac{1}{R}$ between the nodes according to Figure 4.8.

Name	Linked Components	Geometry		
Wheel Fork	Node₁ ↔ Node₂			
	$CON_{10} = \left(\frac{1}{CON_{F1}} + \frac{1}{CON_{F2}} \right)^{-1}$			
	$CON_{10} = 1.46 \cdot 10^{-1} \frac{\text{W}}{\text{K}}$			
Part	Cross section	Length	Material	Amount
Fork 1	$S_{F1} = 200 \text{ mm}^2$	$l_{F1} = 175$	Aluminium	1
Fork 1	$S_{F2} = 200 \text{ mm}^2$	$l_{F2} = 175$	Aluminium	1

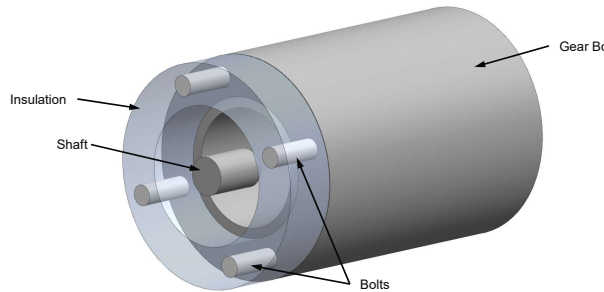
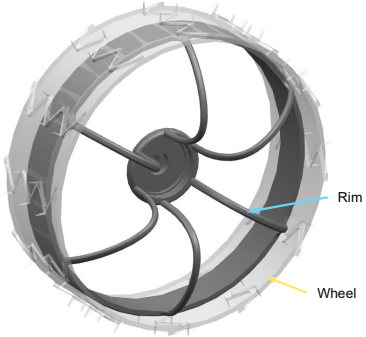
Name	Linked Components	Geometry		
Mounting	Drive Engine ↔ Node₂			
	$CON_{11} = \left(\frac{1}{CON_G} + \frac{1}{CON_S + CON_I + n_B \cdot CON_B} \right)^{-1}$			
	$CON_{11} = 2.19 \cdot 10^{-1} \frac{\text{W}}{\text{K}}$			
Part	Cross section	Thickness	Material	Amount
Gear Box	$S_G = 566 \text{ mm}^2$	$t_G = 43.1 \text{ mm}$	Steel	1
Shaft	$S_S = 23.8 \text{ mm}^2$	$t_S = 8 \text{ mm}$	Steel	1
Insulation	$S_I = 490 \text{ mm}^2$	$t_I = 8 \text{ mm}$	Aerogel	1
Bolts, M3	$S_B = 7.07 \text{ mm}^2$	$t_B = 8 \text{ mm}$	Steel	4

Table F.5: Definition of heat conductance $CON = \frac{1}{R}$ between the nodes according to Figure 4.8.

Name	Linked Components	Geometry		
Rim	Node₂ ↔ Ground			
	$CON_{13} = 5.11 \cdot 10^{-3} \frac{\text{W}}{\text{K}}$			
Part	Cross section	Length	Material	Amount
Rim	$S_R = 12 \text{ mm}^2$	$l_r = 100 \text{ mm}$	Aluminium	6

Note: It was assumed, that the wheel temperature equals the surface temperature because of the thin rims and resulting low heat conduction.

F.3 Heat switch

The characteristic of the switch conductance depends on the mean temperature T_M , shown by measurements in cite . As this temperature won't be calculated in the analysis, the corresponding component temperature T_C shall be used. In order to describe the characteristic, it was divided in three sections, Figure F.1. The temperature where the disk decouples is $T_{toggle} = 108K$ and not applicable for the current application. By reducing the height, the toggle temperature can be increased and the characteristic can be shifted to higher temperatures ("to the right"). It was assumed, that the gradients of section 2 and 3 as well as the temperature range of section 2 keep constant. The axis intersection is a function of the toggle temperature ($a_2 = f(\Delta T_{toggle})$, $\Delta T_{Toggle} = T_{new} - T_{old}|_{toggle}$). The used toggle temperature are listed in autoref

F. THERMAL CONTROLS SYSTEM

Table F.6: Sections and range of the switch characteristic.

Section	Temperature range	Heat conductance $CON_S = \frac{1}{R_t}$
1	$T_{toggle} > T_C$	$CON_S = 16.4 \cdot 10^{-3} \frac{\text{W}}{\text{m}^2\text{K}} = const.$
2	$T_{toggle} \leq T_C < T_1$	$CON_S(T_C) = a_{1.1} \cdot T_C + a_{1.2}$ $a_{1.1} = +1.272 \cdot 10^{-3} \frac{\text{W}}{\text{m}^2\text{K}^2}$ $a_{1.2} = -1.272 \cdot 10^{-3} \frac{\text{W}}{\text{m}^2\text{K}^2} \cdot \Delta T_{Toggle} - 0.117 \frac{\text{W}}{\text{m}^2\text{K}}$
3	$T_C > T_1$	$CON_S(T_C) = a_{2.1} \cdot T_C + a_{2.2}$ $a_{2.1} = +333 \cdot 10^{-6} \frac{\text{W}}{\text{m}^2\text{K}^2}$ $a_{2.2} = -333 \cdot 10^{-6} \frac{\text{W}}{\text{m}^2\text{K}^2} \cdot \Delta T_{Toggle} - 28.3 \cdot 10^{-3} \frac{\text{W}}{\text{m}^2\text{K}}$

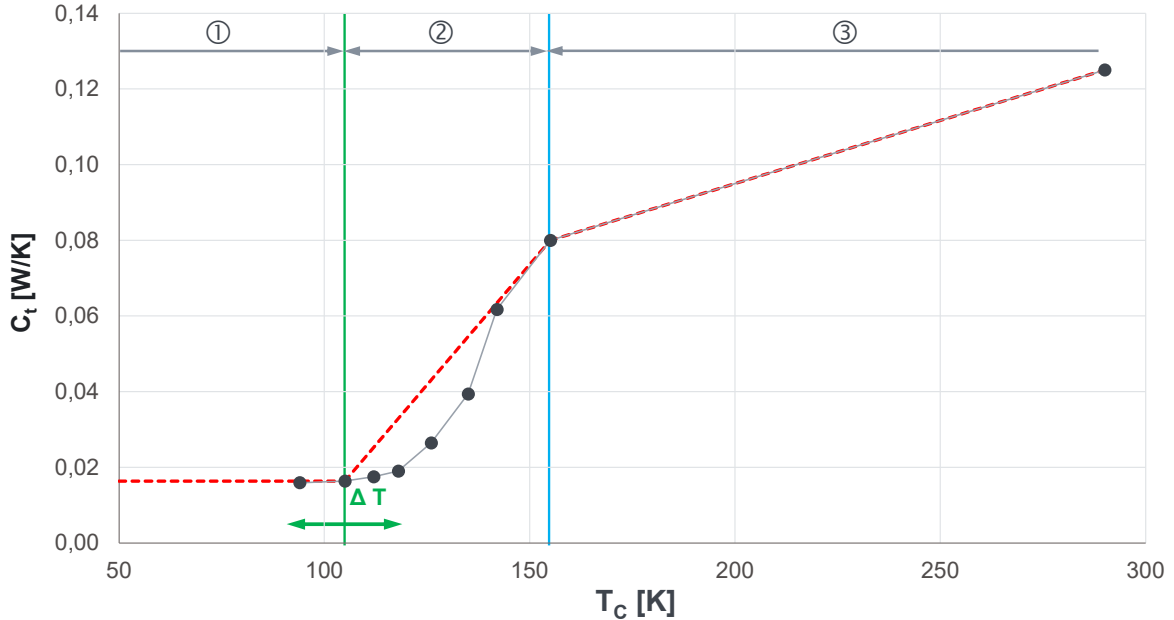


Figure F.1: Conductance characteristic of heat switch diveded in sections.

Table F.7: Toggle temperature and amount of bi-metallic heat switch.

Heat switch name	Linked Components	Temperature	Amount
CON_{S1}	Camera \leftrightarrow Radiator	-20 °C	$n_{S1} = 4$
CON_{S2}	EBay \leftrightarrow Chassis	-30 °C	$n_{S2} = 2$
CON_{S3}	Drive Engine \leftrightarrow Node2	-20 °C	$n_{S3} = 1$ (in total 4)

F.4 Rover absorptivity

The rover position relativ to the direct sun radiation is given by the ecliptic longitude λ_R and latitude δ_R angle, where the axis x_E points always to the sun, Figure F.2b. The amount of solar radiation S_0 absorbed by the rover surfaces depends on the sun altitude and can be determined by the view factor φ , see Figure F.2a. The view factors during eclipse are set to zero.

$$\text{View Factor 1, horizontal surface: } \varphi_1 = \cos(\lambda_R) \cdot \cos(\delta_R)$$

$$\text{View Factor 2, vertical surface: } \varphi_2 = \cos(90^\circ - \lambda_R) \cdot \cos(\delta_R)$$

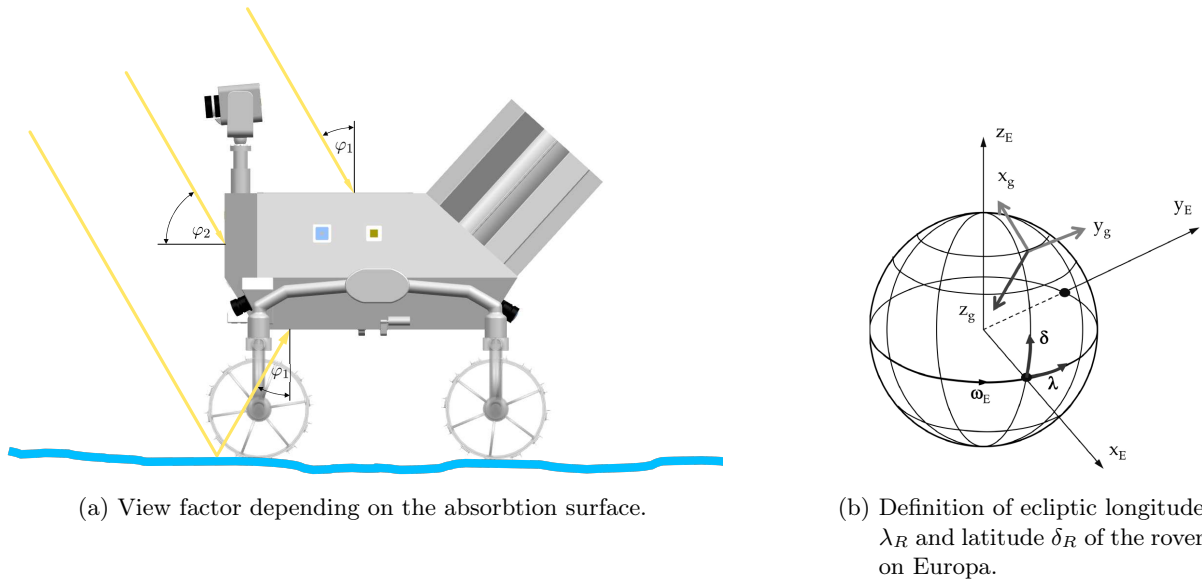


Figure F.2: Bi-metallic heat switch, [20].

F.5 Input Values

Table F.8: Temperatur limits of the rover components.

Component	Temperature limits in [°C]		Source
	min.	max.	
OBC	-55	70	
Transmitter	-10	50	
Receiver	-30	70	
PCDU	-40	60	
Battery	-20	60	[14]
Camera	-40	70	
Objektive	-40	71	
Steering Engine	-30	100	
Drive Engine	-40	100	
Drive Gear	-40	100	

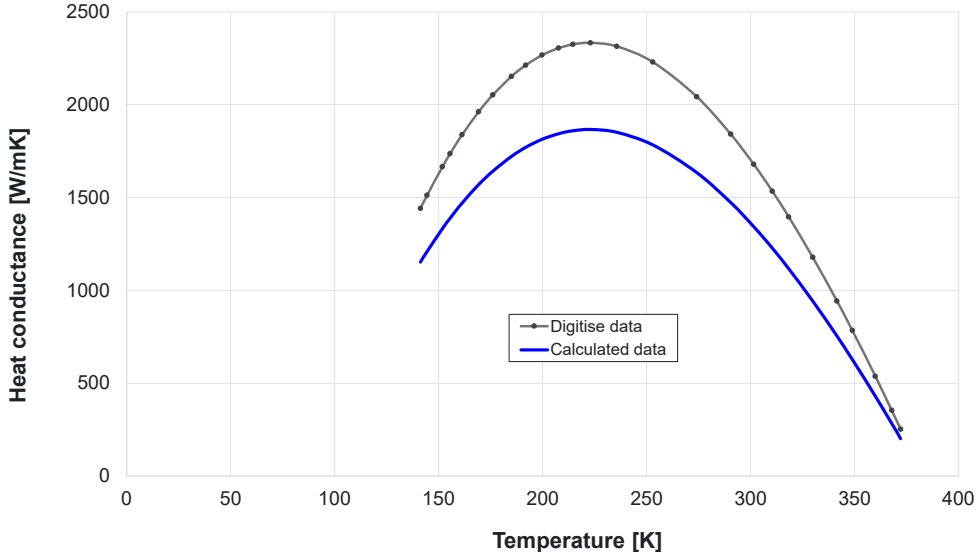


Figure F.3: Digitalised [17] and calculated heat conduction in comparison.

The characteristic of the *LyNX®* conduction was approximated with following function,

$$\lambda(T) = \left(1.76 \cdot 10^{-4} \frac{\text{W}}{\text{mK}^4} \cdot T^3 - 2.37 \cdot 10^{-1} \frac{\text{W}}{\text{mK}^3} \cdot T^2 + 79.5 \frac{\text{W}}{\text{mK}^2} \cdot T - 5.55 \cdot 10^3 \frac{\text{W}}{\text{mK}} \right) \cdot f_r \quad (5.14)$$

with the reduction factor $f_r=0.8$.

Table F.9: Dimensions of the thermal straps *LyNX®*.

Linked Components	Cross section	Length ¹⁾
EBay \leftrightarrow RTG	42 mm ²	230 mm
Drill \leftrightarrow RTG	10 mm ²	345 mm
Steer Engine \leftrightarrow RTG	36 mm ²	644 mm
Drive Engine \leftrightarrow RTG	42 mm ²	897 mm

¹⁾ Due to uncertainties the length was increased about 15%.

The Europa surface temperature varies at the equator between $T_{e,min} = 80$ K and $T_{e,max} = 130$ K, depending on the sun inclination. The temperature at the pole is $T_{Pole} = 50$ K, [16]. It was assumed, that the surface temperature depends on the sun altitude. A trigonometrical interpolation was defined as follows.

$$T_{Surface}(\lambda, \delta) = T_{Pole} + \cos(\delta) \cdot [(T_{e,min} + \cos(\lambda) \cdot (T_{e,max} - T_{e,min})) - T_{Pole}]$$

For λ and δ see Subsection F.4.

Table F.10: Minimum and maximum of surface emisivity and absorptivity values, [21].

Surface finishing	Emisivity [-]		Absorptivity [-]	
	min.	max.	min.	max.
Aluminium, polished		0.05		0.2
Aluminium, sand blasted		0.2		0.4
White paint	0.8	0.9	0.2	0.5

 Table F.11: Heat conductivity in $\frac{\text{W}}{\text{mK}}$

Material	Nominal	Used	Source
Aerogel	0.002 - 0.05	0.05	[19]
Aluminium ¹⁾	110 - 220	220	[22], [23], [24]
Steel ¹⁾	15 - 43	45	[25], [26]
Titan	7.1	7.1	[27], [28]

¹⁾ Depends on the alloying component, a conservative value was choosen.

Table F.12: Radiation surface and finishing of components.

Part	Surface [m^2]	Finishing	Note
Chassis - top/bottom	$S_{Ch1} = 0.086$	white paint	for albedo
Chassis - side	$S_{Ch2} = 0.081$	white paint	for albedo
Chassis - total	$S_{Ch3} = 0.423$	white paint	for emisivity
RTG	$S_{RTG} = 0.086$	white paint	konstant emisivity of 0.9
Electric Bay	$S_{Bay} = 0.146$	aluminium, sand blastet	
Camera - housing	$S_{Cam} = 0.027$	aluminium, sand blastet	
Camera - radiator	$S_{Rad} = 0.066$	white paint	
Steer Engine	$S_{E,S} = 0.002$	white paint	
Drive Engine	$S_{E,D} = 0.003$	white paint	
Bogie	$S_B = 0.018$	white paint	
Wheel Fork	$S_F = 0.008$	white paint	

The cross sections were taken form the CAD model.

G Radiation

In this chapter, detailed calculations are performed on which Section 4.6 is based on. All calculations and figures in Section G are performed with SPENVIS unless otherwise stated. In order to simulate the radiation on Europa an orbit around Jupiter is simulated with the orbit parameters of Europa with a total mission duration of 30 days. The chosen parameters were an perijove altitude of 664,862 km, an apojove altitude of 676,938 km, and an inclination of 0.47°.

G.1 Jupiters Radiation Environment

In order to compare the radiation environment around Jupiter and the radiation environment around Earth the following trapped radiation models were used: for Jupiter the D&G83+Salammbo proton model and D&G83+GIRE+SalammboE electron model was used; for Earth the AP-8 proton model and the AE-8 electron model was used.

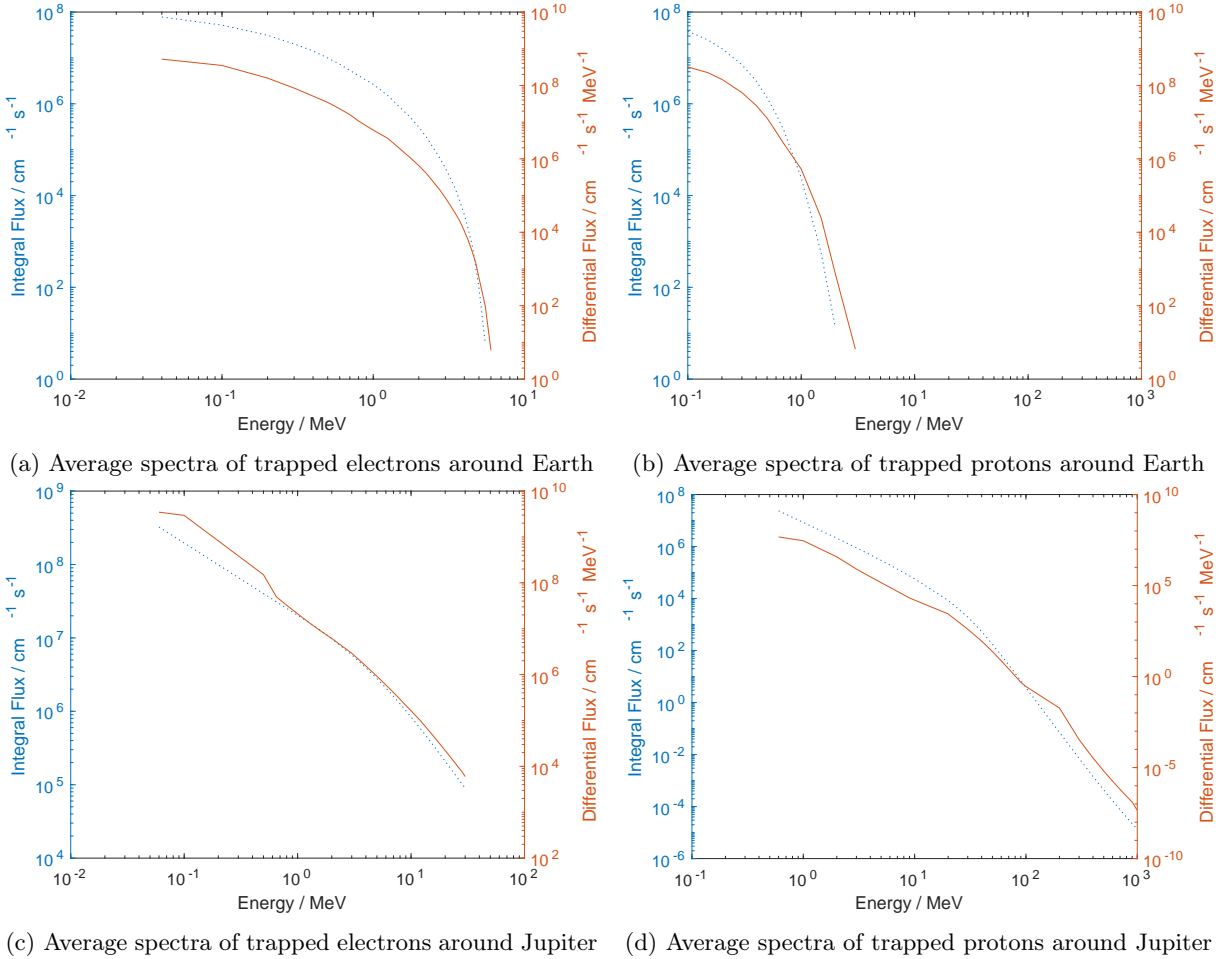


Figure G.1: Average trapped proton and electron fluxes on an orbit around earth at 25,000 km, through the outer Van Allen radiation belt, and on Europa's orbit around Jupiter.

G.2 Radiation Exposures

In order to simulate the TID for different radiation protections the Geant4 tool Multi-Layered Shielding Simulation (MULASSIS) is used. As target material silicon is selected with a thickness of 1 μm . As shape a planar slab is selected because of the ice ground on one side of the rover.

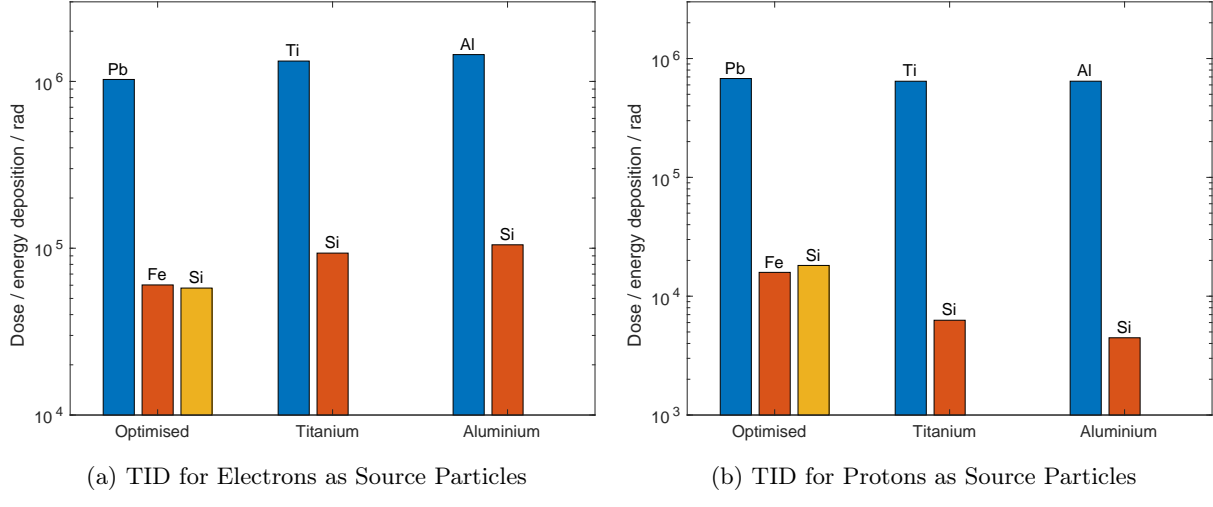


Figure G.2: TID of aluminium, titanium, and the optimised radiation structure shown in Table 4.8 with a weight target of all three structures of 0.5 g/cm^2 over 30 days of exposure on Europa.

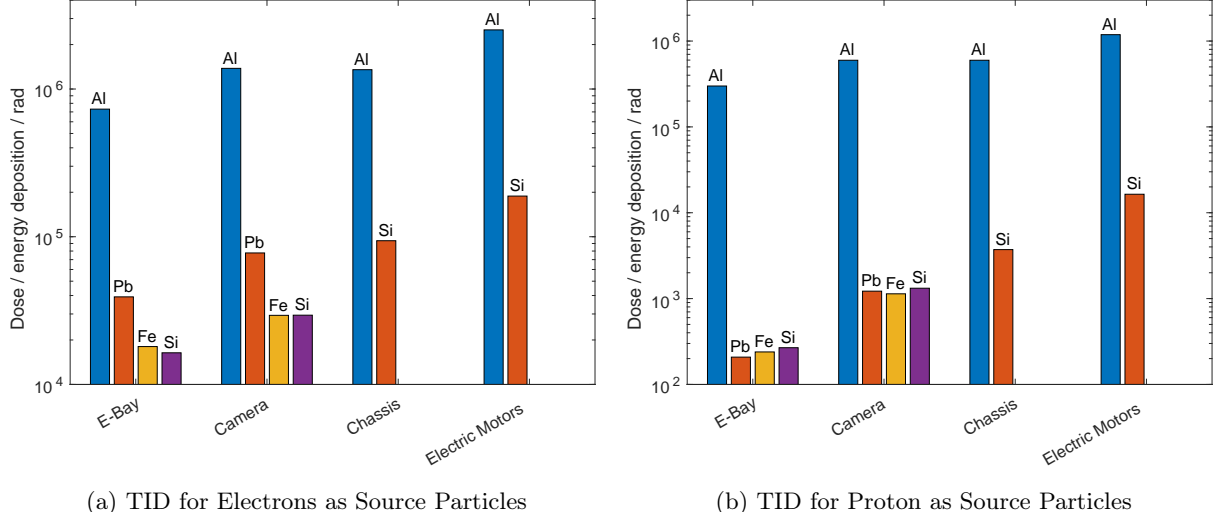


Figure G.3: TID for different compartments as seen in Figure 4.9. The E-Bay is shielded by 4 mm aluminium, 0.415 mm lead, and 0.033 mm iron; the camera compartment by 2 mm aluminium, 0.415 mm lead, and 0.033 mm iron; the chassis by 2 mm aluminium; the electric motors by 1 mm aluminium.

Table G.1: Used components and the respective radiation tolerance and location

Components	Rated TID	Exposed TID	Location
BLDC Motors	-	< 205	locomotion housing
Stepper Motors	100 000	< 205	locomotion housing
Harness	-	< 98	chassis
Stereo Vision Cams	40	< 31	camera housing
OBC	1000	< 17	E-Bay
PCDU	20	< 17	E-Bay
Transmitter	20	< 17	E-Bay
Receiver	20	< 17	E-Bay
Battery	20	< 17	E-Bay
Housekeeping Board	≈ 20	< 17	E-Bay
IMU	≈ 20	< 17	E-Bay
Multiplexer	≈ 20	< 17	E-Bay
Ground Radar	≈ 20	< 17	E-Bay
Sun Sensor	10 000	2 000	outside rover
Camera Lenses	10 000	2 000	outside rover

G.3 Improvements

All simulations of the improvements introduced in Subsection 4.6.3 are performed in the same way as in Subsection G.2.

In Figure G.4, the TID over 30 days within the E-Bay is shown. If all components with a radiation resistance under 43.27 krad are shielded individually, the additional shielding structure around the E-Bay can be removed and the aluminium structure would be sufficient.

The resulting mass savings can be calculated with Equation 5.15 with m^* as the specific weight of the radiation protection and N as the amount of components within the E-Bay with a radiation resistance under 43.27 krad as of Table G.1.

$$\Delta m = SA_{E\text{-Bay}} \cdot m_{\text{Shielding}}^* - \sum_{n=0}^N SA_{\text{Component, n}} \cdot m_{\text{Shielding}}^* \quad (5.15)$$

With inserted values this results in a mass saving of $\Delta m = 736.2$ g.

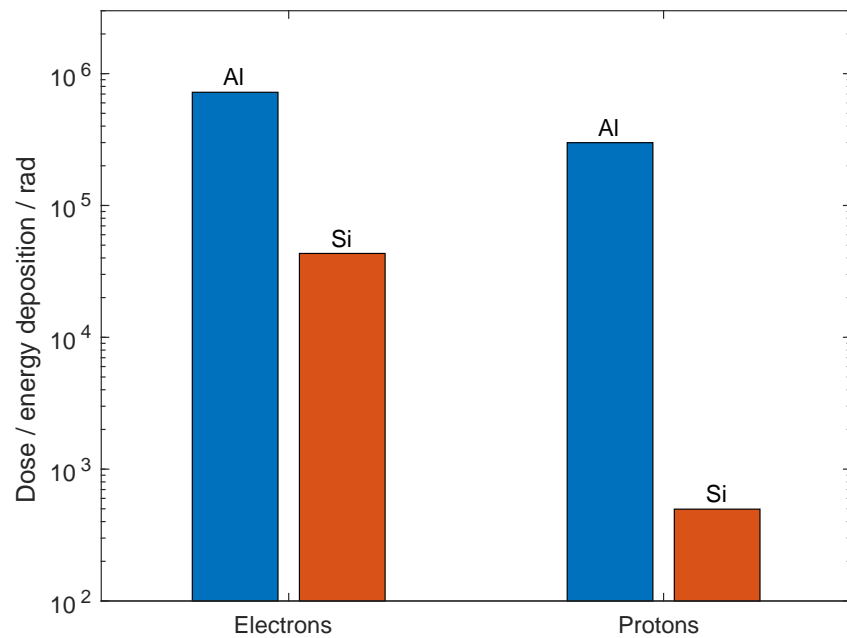


Figure G.4: TID with 4 mm Al shielding over a mission duration of 30 days

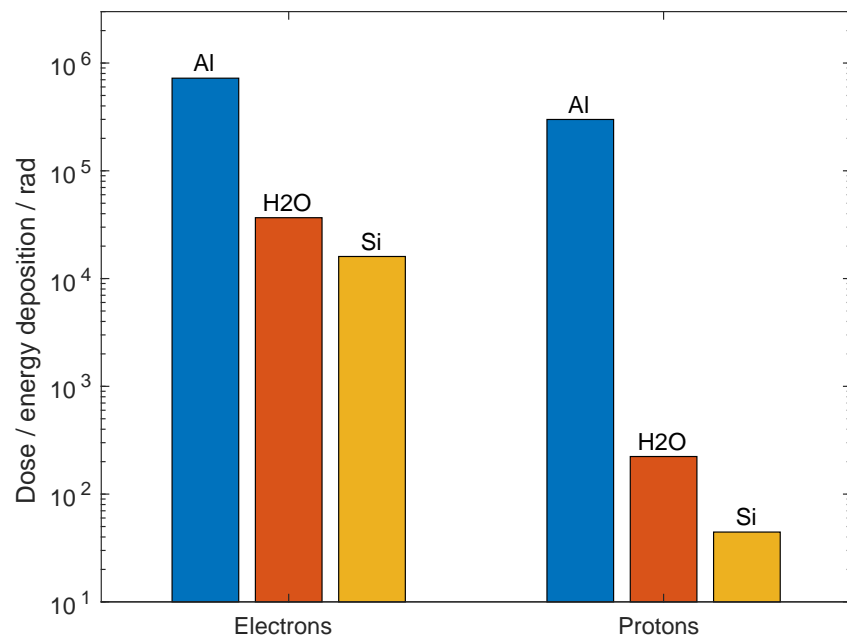


Figure G.5: TID with 4 mm Al shielding and 1 cm of Water over a mission duration of 30 days

H Digital Appendix

Name	Path	Type	Size
TCS Analysis final	300 Thermal	Exle Sheet with Macros, *.xlsm	326 kB

Table H.1: Digital Appendix